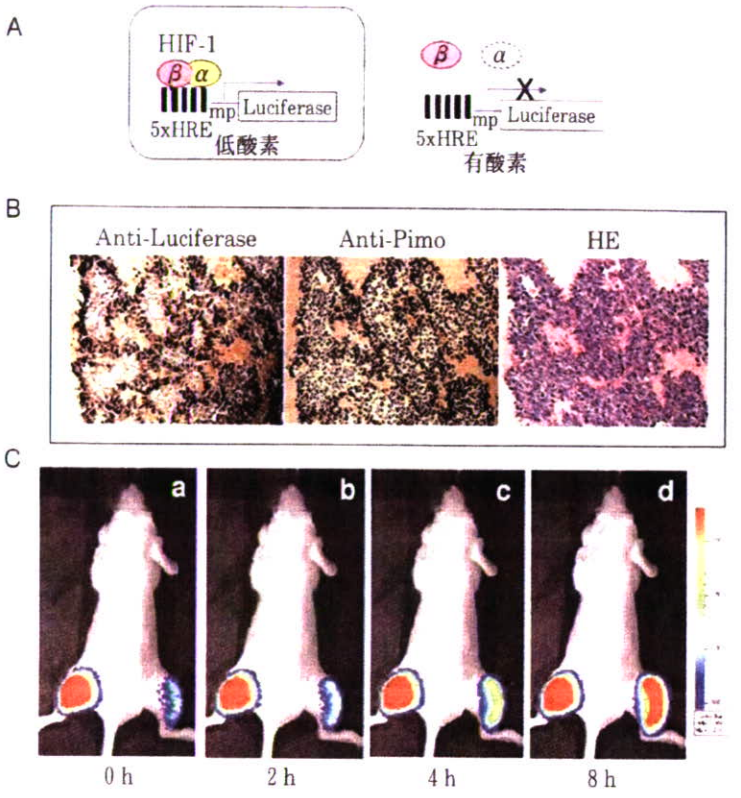


**図4　ルシフェラーゼによる化学発光を用いた低酸素がん細胞の可視化**

A：低酸素応答プロモーター 5HRE は，*VEGF* 遺伝子の低酸素応答エンハンサー(HRE)を並列に 5 個つなげた配列に，哺乳動物細胞で転写活性を有するプロモーターの最小単位（mp：minimum promoter）を組み合わせた構造をしており，5HRE の下流にルシフェラーゼ遺伝子を繋いだレポータープラズミドを体細胞 DNA に安定に組み込んだヒトがん細胞を樹立した。低酸素状態の細胞では，転写因子 HIF-1 が HRE 配列に結合してルシフェラーゼが発現する（左）が，有酸素状態の細胞では，HIF-1α が分解されるため HIF-1 が形成されずルシフェラーゼの発現は起こらない（右）。

B：A で示したがん細胞をヌードマウスに移植して形成した固形腫瘍の連続切片を抗ルシフェラーゼ抗体(左)，抗低酸素マーカー pimonidazole 抗体(中央)で免疫染色した。生細胞と死細胞を識別するために HE 染色（右）を行ったところ，ルシフェラーゼの発現している領域が低酸素マーカーで染色された領域(ともに濃い茶色）がほぼ一致し，更に生細胞と死細胞の境界領域に位置しており，ルシフェラーゼの発現領域が低酸素がん細胞であることが確認できた。

C：B の固形腫瘍がある右足の付け根を紐でしばって血流を下げることで，腫瘍内の低酸素領域を増やした場合のルシフェラーゼの発現増加過程をしらべるために，ルシフェリンとの反応による化学発光を *in vivo* イメージングシステムで経時的（結紮直後，2，4，8 時間後）に調べた。

る。事実，ヒトがんから採取された生検サンプルを，抗 HIF-1α モノクローナル抗体を用いた免疫染色を行うことで，脳腫瘍，乳がん，中咽頭がん，子宮頸がん，卵巣がん，子宮がんを含む大多数のヒトがんにおいて HIF-1α が過剰発現しており，HIF-1α の過剰発現と患者の死亡率に相関関係があることが報告されている（文献 5，6 参照）。病理的な解析で進行癌のステージが低くても，HIF-1α の発現が高い場合は，死亡率が

高いという報告もある。腫瘍内の HIF-1α の過剰発現を引き起こす要因としては，低酸素，遺伝子変異，増殖因子等が挙げられる。したがって，HIF-1 の活性を抑制することで，がんの増殖を抑制し，悪性度を下げることができると考えられ，これまでに様々な試みがなられており，動物実験レベルでも HIF-1 活性を抑えることが抗がん治療に非常に有効であることが報告されている。

### 1．シグナル伝達阻害剤

現在 HIF-1α の発現レベルを抑える作用がある抗がん剤として挙げられているのは，前述した HIF-1α 翻訳レベルを上昇させる PI3K-AKT-mTOR や RAF-MEK-ERK シグナル伝達阻害剤である（**図 3**，文献 5，6 参照）。BAY 43-9006（RAF），CCI-779（mTOR），Celebrex® （COX2），PD98059（MEK），Herceptin® （Tyrosine kinease），Iressa® （Tyrosine kinease），Glivec® （Tyrosine kinease）が例として挙げられる。しかしながらこれらの抗がん剤は，標的が HIF-1α 以外であるため結果的に HIF-1α の翻訳レベルが低下しているが，そのことがこれらの抗がん効果にどれくらい貢献しているかの評価は難しい。

### 2．HIF-1 活性抑制

HIF-1 の活性を抑制している薬剤としては，2-methoxyoestradiol（2ME2），YC-1，topoisomerase I inhibitors，17-AAG，thioredoxin inhibitors が挙げられる（**図 3**，文献 5，6 参照）。2ME2 は micritubule polymerization を壊す作用があり，YC-1 は guaniylate-cyclase 活性を促進する作用があることがわかっているが，HIF-1α の活性が何故抑制されるのかは解明されていない。Topoisomerase I inhibitor も HIF-1α 抑制機構についてはわかっていない。17-AAG は，ER で HIF-1α に結合するシャペロン分子である HSP90 に直接結合して HSP90 の機能を阻害することが分かっており，結果 HIF-1α はユビキチン－プロテアゾーム系による分解とは関係なく分解することが分かっている。Thioredoxin は HIF-1 転写複合体の一員と示唆されている Ref-1/Ape の制御を介して HIF-1 α の発現を促進する作用があり[17]，thioredoxin inhibitor はそれを阻害することで HIF-1 活性を下げている。これらは，いずれも HIF-1α の発現および腫瘍の増殖を抑える作用が報告されている。これらの HIF-1 活性抑制剤もシグナル伝達阻害剤と同様に，HIF-1 に対する特異性という点では明確でなく，上記シグナル伝達阻害剤と同様に HIF-1 活性阻害が，どれくらい抗がん作用に貢献しているかを評価するのは難しい。

### 3．低酸素特異的抗がんタンパク製剤

上記 HIF-1 阻害剤や活性抑制剤は，“分子標的アプローチ”であるのに対し，我々は，いわば“微細環境標的アプローチ”といえる手法を用いて HIF-1 のターゲティングに挑んだ。すなわち HIF-1α と同様の酸素依存的制御を受ける細胞死誘導タンパク質を構築し，低酸素がん細胞を特異的に死滅させるという方法である[18]。任意のタンパク質に，HIF-1α の酸素濃度依存的分解（ODD）ドメイン（PHDs により水酸化される P564 を含む）を任意のタンパク質に融合させると，その融合タンパク質は，HIF-1α と同様の PHDs による翻訳後修飾による制御を受けるようになる（**図 5 A**）。低酸素がん細胞を特異的に殺すため，ODD に融合するタンパク質として，強力なアポトーシス誘導能を有する caspase-3 の前駆体 procaspase-3 を選択した。Procaspase-3 は，過剰発現しても細胞死を誘導することはないが，上流のカスペース等により切断されて活性型になると，死刑執行人と称されるほど，強力に細胞死を誘導する。ODD-procaspase-3 融合タンパク質を血流の悪い腫瘍内低酸素領域までデリバリーさせるために，AIDS ウイルスの TAT タンパク質が有する膜透過ドメイン PTD を融合させた。TAT-PTD は，融合したタンパク質を脳を含む全身の組織細胞ににデリバリーさせることができる[19]。最終的に構築したタンパク質製剤 TOP3（$TAT_{PTD}$-ODD-Procaspase-3）は，PTD による DDS 機能と ODD による低酸素細胞特異性を有する抗がん剤として，培養細胞では低酸素特異的に細胞死を誘導し，動物実験でも抗腫瘍効果を発揮した[3, 16, 18, 20]。上述した低酸素がん細胞をイメージングする方法を用いて，実際に *in vivo* で低酸素がん細胞を標的にしているか否かを検証した結果，TOP3 治療群

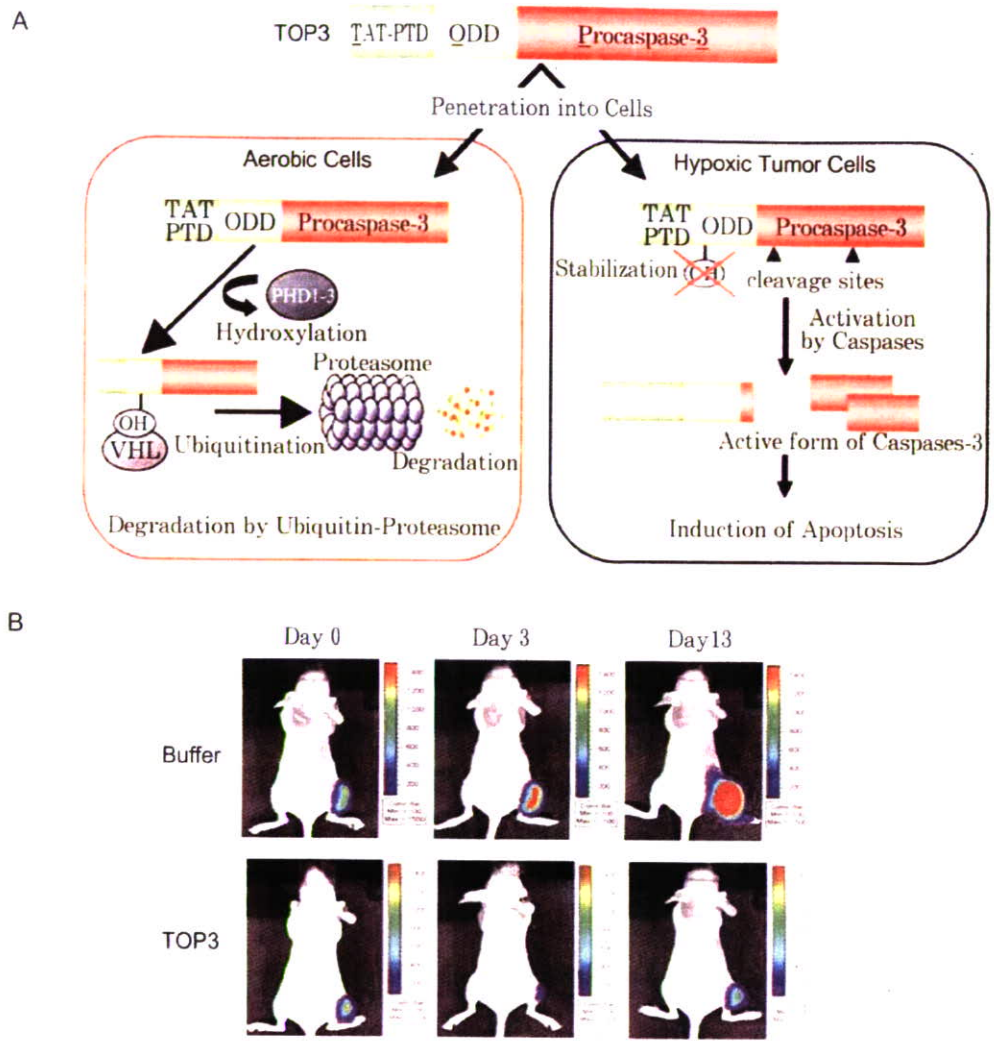


**図5　TOP3の作用機序とTOP3処理による低酸素がん細胞の推移**

A：TOP3の作用機序を模式的に示した。TOP3は，TAT-PTDの機能により細胞膜を通過して細胞内に入り（上），有酸素状態でがHIF-1$\alpha$と同様にユビキチン－プロテアソーム系（図2）で分解される（左）が，低酸素状態では分解されず，低酸素ストレスにより活性化されている内在性のカスパーゼによってProcaspase-3が切断されて活性型Caspase-3になって細胞死を誘導する（右）。

B：下肢に図4Aのレポーターを有する細胞の移植腫瘍を持つ担がんマウスを，TOP3またはBufferで処理して，低酸素がん細胞で発現しているルシフェラーゼの活性を*in vivo*イメージングシステムで毎日観察し，化学発光量（photons/sec/ROI）を計測した。データのうち，day0，3，13における代表的な観察図を示した。

では，顕著に低酸素がん細胞からの発光シグナルが抑えられていることが確認でき，TOP3の*in vivo*での低酸素がん細胞特異的抗がん作用を強く示唆する結果を得た（図5B）。また，経時的に腫瘍の切片を作成して，免疫組織染色法にて固形腫瘍内の低酸素領域を調べた結果，TOP3投与後48時間以内に低酸素領域が顕著に減少していることが確認できた。さらに，TUNELアッセイを行って切片におけるアポトーシスをTOP3投与後12時間で観察したところ，TOP3投与群の腫瘍では，有意に高いTUNEL陽性反応が，生細胞と壊死領域の境界領域に存在し，TOP3は，固形腫瘍内でも低酸素がん細胞にアポトーシスを誘導していることが示唆された[16]。

TOP3処理で，放射線抵抗性を有する低酸素がん細

胞を積極的に腫瘍から排除することにより，放射線治療効果を高めることができるか否かを検証した。TOP3 処理後 1 日目に 15 Gy の放射線を照射した。放射線処理単独でも顕著な抗がん効果が見られたが，TOP3 と併用することで，明らかに腫瘍の再増殖を遅らせることができた。この結果は，TOP3 処理により固形腫瘍から低酸素がん細胞が除去されたためであり，低酸素がん細胞が放射線治療後の再発に寄与していることを支持すると共に，有酸素がん細胞と低酸素がん細胞をほぼ同時に処理することがん療効果を高めることを示していると言える。

## おわりに

動物実験におけるデータであるが，低酸素がん細胞は，腫瘍径が 1 mm 以下でも既に存在することが確認されている。"低酸素あるところには必ず HIF-1 あり" ということであれば，HIF-1 は腫瘍形成の初期から貢献している事になる。分子標的の対象因子と異なり，低酸素は "正常組織には存在しない環境因子" である。従って，HIF-1 の存在する細胞を特異的にイメージング・ターゲティングすることができれば，がんの悪性化に関与する低酸素がん細胞の存在を確認し，攻撃することが可能になる。その点で "環境標的アプローチ" は "HIF-1 の存在する細胞" を標的にするという，極めて特異性の高い，新しい腫瘍へのアプローチを提案しているといえる。

## 文　献


1) Vaupel P, Kallinowski F, Okunieff P : Blood flow, oxygen and nutrient supply, and metabolic microenvironment of human tumors : a review. Cancer Res **49** : 6449-6465, 1989
2) Harris AL : Hypoxia-A key regulator factor in tumor growth. Nature Rev Cancer **2** : 38-47, 2002
3) Kizaka-Kondoh S, Inoue M, Harada H, Hiraoka M : Tumor hypoxia : A target for selective cancer therapy. Cancer Sci **94** : 1021-1028, 2003
4) H ö ckel M, Schlenger K, Aral B et al : Association between tumor hypoxia and malignant progression in advanced cancer of the uterine cervix. Cancer Res **56** : 4509-4515, 1996
5) Semenza GL : Targeting HIF-1 for cancer therapy. Nat Rev Cancer **3** : 721-732, 2003
6) Giaccia A, Siim BG, Johnson RS : HIF-1 as a target for drug development. Nat Rev Drug Discovery **2** : 1-9, 2003
7) Brown JM : Exploiting the hypoxic cancer cell : mechanisms and therapeutic strategies. Mol Med Today **6** : 157-162, 2000
8) Semenza GL, Wang GL : A nuclear factor induced by hypoxia via de novo protein synthesis binds to the human erythropoietin gene enhancer at a site required for transcriptional activation. Mol Cell Biol **12** : 5447-5454, 1992
9) Wang G, Semenza GL : Purification and characterization of hypoxia-inducible factor 1. J Biol Chem **270** : 1230-1237, 1995
10) Ravi R et al : Regulation of tumor angiogenesis by p53-induced degradation of hypoxia-inducible factor 1alpha. Genes Dev **14** : 34-44, 2000
11) Epstein AC et al : C. elegans EGL-9 and mammalian homologs define a family of dioxygenases that regulate HIF by prolyl hydroxylation. Cell **107**(1) : 43-54, 2001
12) Berra E et al : HIF prolyl-hydroxylase 2 is the key oxygen sensor setting low steady-state levels of HIF-1alpha in normoxia. EMBO J **22** : 4082-4090, 2003
13) Mahon PC, Hirota K, Semenza GL : FIH-1 : a novel protein that interacts with HIF-1alpha and VHL to mediate repression of HIF-1 transcriptional activity. Genes Dev **15** : 2675-2686, 2001
14) Vordermark D, Shibata T, Brown JM : Green fluorescent protein is a suitable reporter of tumor hypoxia despite an oxygen requirement for chromophore formation. Neoplasia **3** : 527-534, 2001
15) Serganova I et al : Molecular imaging of temporal dynamics and spatial heterogeneity of hypoxia-inducible factor-1 signal transduction activity in tumors in living mice. Cancer Res **64** : 6101-6108, 2004
16) Harada H, Kizaka-Kondoh S, Hiraoka M : Optical Imaging of Tumor Hypoxia and Evaluation of Efficacy of a Hypoxia-targeting drug in living animals. Mol Imaging : in press
17) Ziel KA et al : Ref-1/Ape is critical for formation of the hypoxia-inducible transcriptional complex on the hypoxic response element of the rat pulmonary artery endothelial cell VEGF gene. FASEB J **18** (9) : 986-988, 2004
18) Harada H, Hiraoka M, Kizaka-Kondoh S : Antitu-

mor effect of TAT-oxygen-dependent degradation-caspase-3 fusion protein specifically stabilized and activated in hypoxic tumor cells. Cancer Res 62 : 2013-2018, 2002
19) Schwarze SR, Ho A, Vocero-Akbani A, Dowdy SF : In vivo protein transduction : delivery of a biologically active protein into the mouse. Science 285 : 1569-1572, 1999
20) Inoue M, Mukai M, Hamanaka Y et al : Targeting hypoxic cancer cells with a protein prodrug is effective in experimental malignant ascites. Int J Oncol 25 : 713-720, 2004

# 『低酸素癌細胞』を標的とした癌のイメージング・ターゲティング

近藤科江，原田　浩，平岡真寛

生体イメージングは，同一個体での癌の進行や治療効果を経時的に観察することを可能にし，治療のうえでのポイントとなる時期の決定を容易にしてくれる．経済性に優れ，動物にも優しい手法である．癌研究では，癌細胞を可視化し，位置や大きさといった物理的情報を得ることが多いが，さまざまな遺伝子発現プロモーターを用いることにより，質的情報も得ることができる．われわれは，癌の悪性度の指標とされる腫瘍内低酸素癌細胞を化学発光で可視化する系を構築し，癌の早期発見・早期治療のために開発中のイメージング・ターゲティング材料の標的特異性評価に用いている．

## はじめに

ルシフェラーゼのレポーターとしての有用性は，培養細胞への一過性発現実験によって示されており，転写因子研究において頻用されてきた．小動物のイメージング機器が開発されて，ルシフェラーゼ活性を個体レベルで測定することが可能になり，培養細胞を用いて行っていた実験が個体レベルで可能な時代になった．具体的には，ルシフェラーゼ・レポーター遺伝子を安定に保持する細胞株を構築し，それをマウスに移植し，移植した細胞から産生される微弱な光（ルミネッセンス）を超高感度CCDカメラにより捉え，さらにソフトウェアによりデジタル処理して可視化する装置を用いて観察する．従来の培養細胞を用いた実験同様，ルシフェラーゼ・レポーター遺伝子につなぐプロモーターを変えることで，移植した細胞からさまざまな情報を得ることができる．さらに，特定の遺伝子のプロモーターの下流にルシフェラーゼをつないだレポーター遺伝子を，全身の体細胞にもつトランスジェニックマウスを構築して，生体における特定の遺伝子の発現する時期や組織・量を調べる研究も行われており，この手法による研究の飛躍的な発展が期待できる．

## 生体の光イメージング

ルシフェラーゼを用いた化学発光は，組織透過性に富む光の条件である波長600 nm以上の光を産生することができ，1 cmを超える透過性をもつため，マウスでは，深い組織内の腫瘍でも，量の推移を経時的に観察することができ，同所移植モデルのように外部からは観察が不可能な癌の研究に有効である（図1）．化学発光イメージングの利点は，高感度性，迅速性および定量性に加えて，何よりも特殊な技術を必要とせず，誰にでも，短時間にイメージを撮ることができる簡便性にある．蛍光物質を用いたイメージングでは，蛍光物質の光安定性や蛍光の組織透過性の問題からリアルタイムで連続的に観察することは難しく，さらに自家蛍光などによるバックグランドの高さから，現行の冷却型CCDカメラを用いたイメージング装置では，蛍光観察に定量性をもたせることは困難である．その一方で，蛍光物質は，ルシフェラーゼのように基質を必要とせず，常時可視化できる点は，一過性の活性を可視化しているルシフェラーゼよりも測定上の誤差が少ない．

現在，蛍光の退色時間を自動的に算出することにより，蛍光を発している細胞

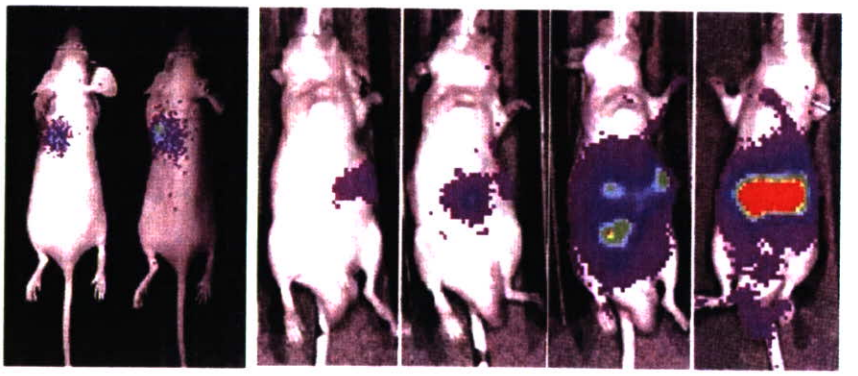


図1●癌の同所移植モデル

（左）ヒトの肺癌細胞をマウスの肺に移植して，肺で増殖した癌細胞を観察．（右）ヒトの膵臓癌細胞をマウスの膵臓に移植し，癌が膵臓から腹膜播種に移行する様子を観察．化学発光が強いところは，赤色に，少なくなるにつれて黄，緑，青，紫に表示される（IVIS®200にて撮影）

の位置や大きさをほぼ正確に三次元で画像化するソフトを搭載しているイメージング機器や，自家発光を波長の違いで画像処理し，バックグラウンドをほぼ完全に除いてイメージングする装置が開発されている．また，700 nm を超え近赤外に近い波長をもつ蛍光プローブも開発されており，将来的には多種多様にある蛍光タンパク質を使い分けて，多重染色により1つの腫瘍から複数の情報を同時に得ることが可能になると考えられる．

個体レベルで癌細胞を画像化する方法としては，放射線同位元素を用いたPETや磁性体を用いたMRIなどの方法が主流であるが，少なくともマウスにおいては，光イメージングが簡便性と経済性において，PETやMRIよりも優れており，これからプローブが多彩になっていくことにより，得られる情報量もPETやMRIを凌ぐものになると思われる．ただし，現状では，光プローブには透過性に限界があり，大型動物やヒトへの応用は現時点では難しく，臨床への応用は，体表面に近い癌や，術中観察に限定されると思われる．

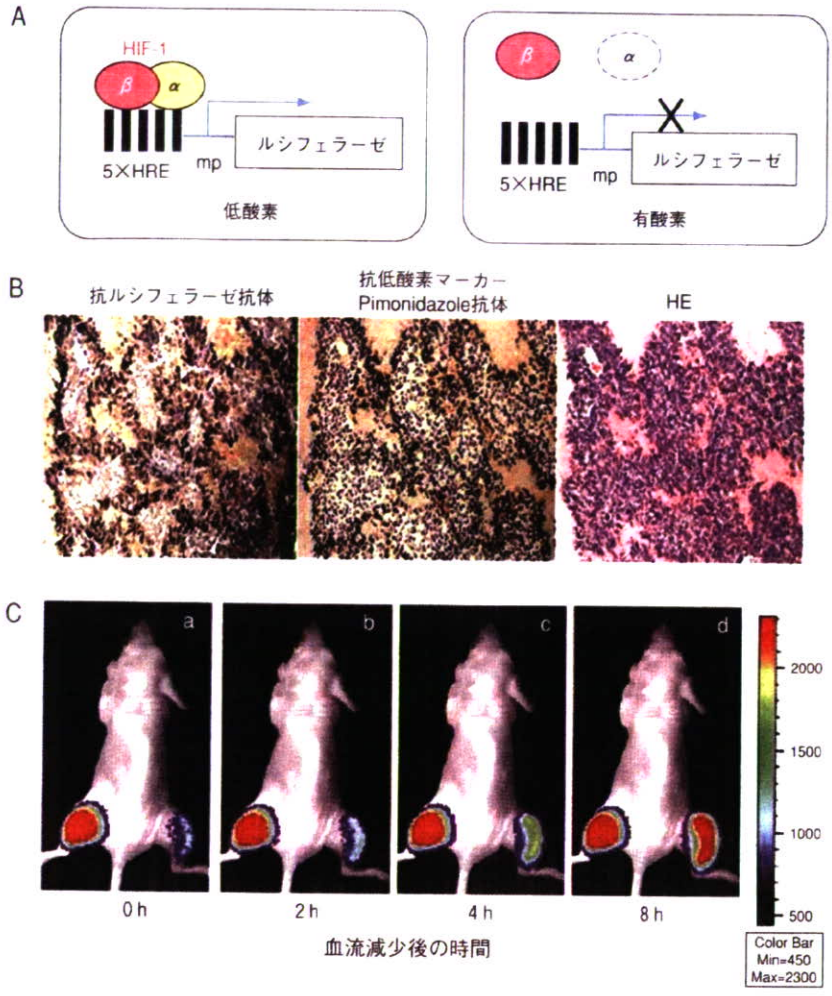


**図2●ルシフェラーゼによる化学発光を用いた低酸素癌細胞の可視化**

A）5HRE-ルシフェラーゼレポータープラズミドを体細胞DNAに安定に組み込んだヒト癌細胞．低酸素状態の細胞では，転写因子HIF-1がHRE配列に結合してルシフェラーゼが発現する（左）が，有酸素状態の細胞では，HIF-1αが分解されるためHIF-1が形成されずルシフェラーゼの発現は起こらない（右）．mp：mininum promoter．B）Aで示した癌細胞をヌードマウスに移植して形成した固形腫瘍の連続切片を抗ルシフェラーゼ抗体（左），抗低酸素マーカーPimonidazole抗体（中央）で免疫染色した．生細胞（紫色）と死細胞（桃色）を識別するためにHE染色（右）を行ったところ，ルシフェラーゼの発現している領域が低酸素マーカーで染色された領域（ともに濃い茶色）と一致しており，ルシフェラーゼの発現領域が低酸素癌細胞であることが確認できた．C）Aの癌細胞を移植して作った固形腫瘍がある右足の付け根を紐でしばって血流を下げることで，腫瘍内の低酸素領域を増やし，ルシフェラーゼの発現を経時的（結紮直後，2，4，8時間後）に調べた．左足の腫瘍は，イメージング操作の誤差を防ぐためのコントロールで，左足のイメージが実験を通して一定になるように画像処理をした

## 微小環境標的

癌に対する治療は，特定の癌に特徴的な分子を標的にした治療薬，いわゆる『分子標的治療薬』の研究開発により，大きな成果をあげている．一方で，どこにできるかわからない癌を早期に発見・治療するためには，癌に共通して存在し，かつ正常組織には存在しない特徴を標的にする必要がある．固形癌に共通して存在する低酸素領域は，正常組織には存在しないため，最適な標的と考えられる．特定の分子を標的にする『分子標的』に対して，われわれの標的は「微小環境標的』といえる．悪性度の高い癌でより多く含まれているとされる低酸素領域は，1 mm以下の微小な癌にも存在するといわれており，初期の癌や転移癌の早期発見のための良い標的になりうる．われわれは，『微小環境標的』のための基礎的材料を，まず光イメージングを用いて開発・評価し，PETやMRIといった臨床応用可能なものの開発に繋げる計画である．

## 低酸素癌細胞とHIF-1

腫瘍内部には，酸素も栄養も枯渇して壊死した細胞領域がある．その周辺の癌細胞は，栄養や酸素が不足しているため，増殖を停止したり，解糖系代謝を行ったりして，何とか生きているが「死ぬべき運命にある弱った癌細胞」である．これ

らの癌細胞（低酸素癌細胞）は，「瀕死状態」ではあるが，その劣悪な環境に適応しようと努力している．その努力の一翼を担っているのが低酸素応答転写因子HIF-1である[1]．通常の酸素濃度にある細胞内では活性が認められないHIF-1は，低酸素条件下ですみやかに活性化され，糖代謝や糖輸送に関与する遺伝子の発現を誘導したり，血管新生因子や増殖因子の産生を促したりして，栄養環境の改善を図る．アポトーシスの回避や，遺伝子変異を引き起こす遺伝子の発現を誘導して，死を免れようとする．その一方で，転移や浸潤にかかわる遺伝子の発現を誘導して，自ら新天地を切り開こうとする．このような一連の「生き残り」のための行動が，実は癌全体の悪性化に繋がっていたのである[1)-3)]．

## HIF-1活性の可視化

以上のように，固形腫瘍内のHIF-1活性は，癌治療，特に難治性の癌において，きわめて重要な因子であり，抗癌治療効果を高め，再発・悪性化を予防するためには，固形腫瘍内のHIF-1活性の分布を明確にすることが重要である．HIF-1によって活性化される遺伝子のプロモーター/エンハンサー領域には，HIF-1が直接結合する配列HRE（hypoxia responsive element）が存在する．われわれは，5個のHREをもつプロモーターの下流にルシフェラーゼ遺伝子をつないだレポータープラズミド（5HRE-Luciferase）[4)]を安定に保持するヒト癌細胞株を樹立している（図2-A）．

これらの癌細胞をヌードマウスに移植すると，形成した腫瘍内の低酸素領域でルシフェラーゼタンパク質が発現され（図2-B），基質であるルシフェリンを投与後一定期間，発光反応を起こす．この化学発光を，冷却高感度CCDカメラを搭載したリアルタイム *in vivo* イメージング装置IVIS™を用いて可視化している．つまり，このシステムを用いることにより，同一担癌マウスの固形腫瘍内低酸素領域の変化を，リアルタイムで，何度でも経時的に観察することが可能である[5)]．しかも発光シグナルを定量することにより，低酸素癌細胞の増減を数量化して推移を観察することができる．この系が腫瘍内の低酸素状態をモニターしていることを確認する目的で，腫瘍を形成した下肢を縛り血行を悪くして，物理的に低酸

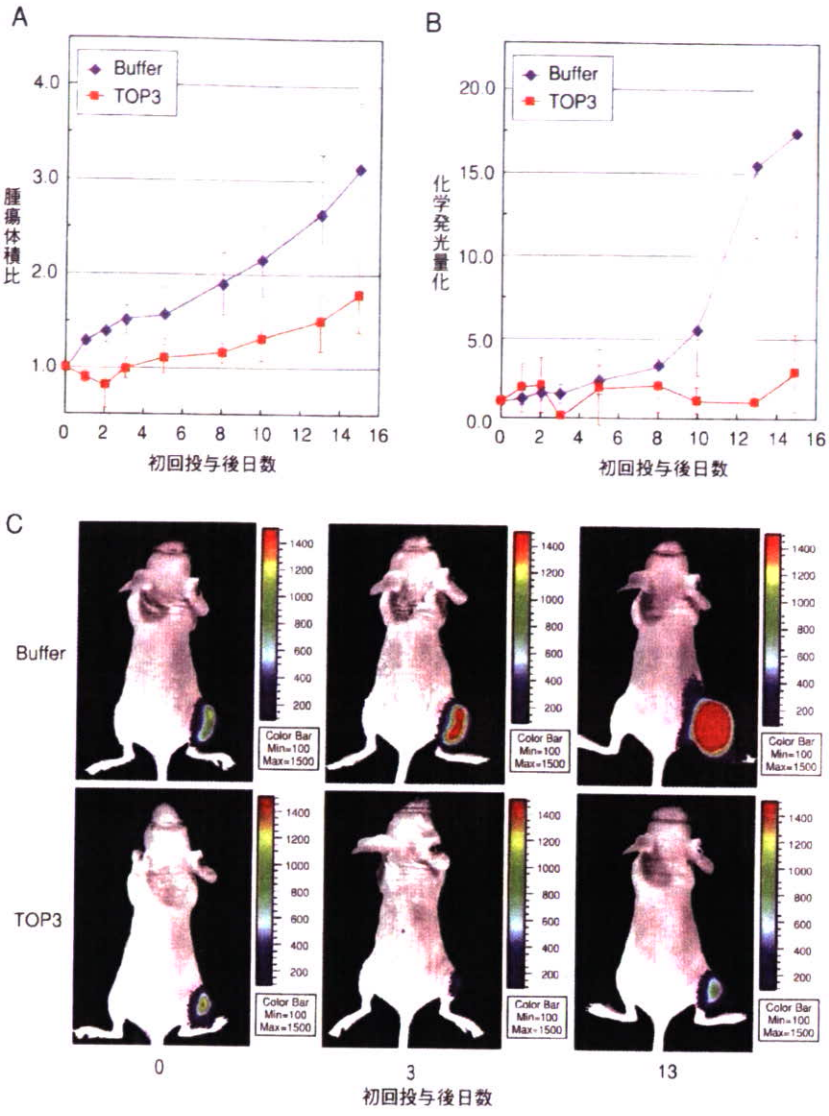


**図3●固形腫瘍内低酸素癌細胞の推移と治療効果の検証**

A）図2-Aの固形腫瘍をTOP3またはBufferで5日おき（0日，5日，10日）に処理して，腫瘍の大きさを計測し，0日との大きさの比でグラフに示した．B）Aの計測と同時にリアルタイムイメージングシステムで化学発光量（photons/sec/ROI）を計測し，0日の化学発光量との比でグラフに示した．C）Bのデータのうち，0日，3日，13日における平均的な画像を示した

素領域を増やす操作をすると，腫瘍内のルシフェラーゼ発現は，結搾時間が経過するとともに上昇した（図2-C）．この結果は，HIF-1が活性化している細胞を可視化することにより，われわれのイメージング・ターゲティングのための『微小環境標的』を可視化できていることを意味している．

## 低酸素特異的融合タンパク質の構築

HIF-1は，αとβの2つのサブユニットから構成されている．HIF-1αは，酸素依存的なユビキチン化を受けて，有酸素状態の細胞内では，翻訳後すみやかに分解される[6]．HIF-1が活性化している細胞を特異的に捕らえるために，われわれは，HIF-1の低酸素依存的活性を制御しているHIF-1αと同じ酸素依存性をもつ融合タンパク質を構築した．具体的には，HIF-1αタンパク質のほぼ中央にある酸素依存的分解ドメイン（oxygen-dependent degradation domain：ODD）内のコアになるアミノ酸配列を任意のタンパク質に融合させると，そのODD融合タンパク質は，HIF-1αと同様に，有酸素状態の細胞ではすみやかに分解され，低酸素状態の細胞では安定に存在する．つまり，ODDを融合させることによって，タンパク質がもつ機能を酸素依存的に制御できるようになる[7]．例えば，融合するタンパク質にイメージング機能をもたせることにより，低酸素癌細胞をイメージングするプローブを作ることができる．

## 低酸素癌細胞のターゲティング

低酸素癌細胞をターゲティングするために，ODDに細胞死誘導タンパク質として，強力なアポトーシス誘導能を有するcaspase-3の前駆体procaspase-3を選択した[7]．*in vivo*でのデリバリー能をもたせるために，AIDSウイルスのTATタンパク質が有する膜透過ドメインPTD（protein transduction domain）を融合させた．TAT-PTDは，融合したタンパク質を脳を含む全身の組織細胞にデリバリーさせることができる[8]．最終的に構築したタンパク質製剤TOP3は，PTDによるDDS機能とODDによる低酸素細胞特異性を有する抗癌剤として，培養細胞では低酸素特異的に細胞死を誘導し，動物実験でも抗腫瘍効果を発揮した（図3-A）[3,5,7,9]．上述した低酸素癌細胞をイメージングする方法を用いて，実際に*in vivo*で低酸素癌細胞を標的にしているか否かを検証した結果，TOP3治療群では，顕著に低酸素癌細胞からの発光シグナルが抑えられていることが確認でき（図3-B，C），TOP3が*in vivo*で低酸素癌細胞特異的抗癌作用をもつことを強く示唆する結果を得た．現在，低酸素特異的イメージングプローブの作製を行っており，少なくとも光イメージングでは，低酸素癌を捕らえることができるところまで来ている．

## おわりに

光イメージングの簡便性は，将来「ベッドサイドでの画像診断」といった夢のような話を実現させてくれる可能性をもっている．それを実現するためには，光の透過性を革新的に高める技術や，機械の感度を上げ，バックグラウンドをなくす機器の開発など，さらなる研究が必要である．より波長の長い蛍光プローブの開発やより強い化学発光基質の探索など，問題解決のための研究は続けられている．機器開発も日進月歩で，多くの研究者の努力が注がれている．夢が現実になる日も，そう遠くないかもしれない．

### 参考文献


1）Semenza, G. L.：Nature Rev. Cancer, 3：721-732, 2003
2）Harris, A. L.：Nature Rev. Cancer, 2：38-47, 2002
3）Kizaka-Kondoh, S. et al.：Cancer Sci, 94：1021-1028, 2003
4）Shibata, T. et al.：Gene Ther., 7：493-498, 2000
5）Harada, H. et al.：Mol. Imaging, 4（3）：182-193, 2005
6）Semenza, G. L.：Cell, 107：1-3, 2001
7）Harada, H. et al.：Cancer Res., 62：2013-2018, 2002
8）Schwarze, S. R. et al.：Science, 285：1569-1572, 1999
9）Inoue, M. et al.：Int. J. Oncol., 25：713-720, 2004



**近藤科江（Shinae Kondoh）**

京都大学大学院医学研究科放射線腫瘍学・画像応用治療学，COE助教授．
1989年に大阪大学微生物病研究所で医学博士課程を修了後，日本学術振興会特別研究員，新技術事業団「岡山細胞変改プロジェクト」研究員，京都大学医学研究科助手を経て，2004年から現職．『癌化機構の解明』のための研究を長年培養細胞で行っていたが，生体イメージングに魅せられて，癌のイメージング・ターゲティング研究に埋没中．

**原田　浩（Hiroshi Harada）**

京都大学大学院医学研究科放射線腫瘍学・画像応用治療学，特任助手

**平岡真寛（Masahiro Hiraoka）**

京都大学大学院医学研究科放射線腫瘍学・画像応用治療学，教授．

# Therapeutic Effects of a $^{186}$Re-Complex–Conjugated Bisphosphonate for the Palliation of Metastatic Bone Pain in an Animal Model

Kazuma Ogawa[1,2], Takahiro Mukai[1,3], Daigo Asano[1], Hidekazu Kawashima[1], Seigo Kinuya[4], Kazuhiro Shiba[2], Kazuyuki Hashimoto[5], Hirofumi Mori[2], and Hideo Saji[1]

*[1]Department of Patho-Functional Bioanalysis, Graduate School of Pharmaceutical Sciences, Kyoto University, Kyoto, Japan; [2]Division of Tracer Kinetics, Advanced Science Research Center, Kanazawa University, Kanazawa, Japan; [3]Department of Biomolecular Recognition Chemistry, Graduate School of Pharmaceutical Sciences, Kyushu University, Fukuoka, Japan; [4]Department of Biotracer Medicine, Graduate School of Medical Sciences, Kanazawa University, Kanazawa, Japan; and [5]Japan Atomic Energy Agency, Tokai-mura, Ibaraki, Japan*

Previously, based on the concept of bifunctional radiopharmaceuticals, we developed a highly stable $^{186}$Re-mercaptoacetylglycylglycylglycine (MAG3) complex–conjugated bisphosphonate, [[[[(4-hydroxy-4,4-diphosphonobutyl)carbamoylmethyl]carbamoylmethyl]carbamoylmethyl]carbamoylmethanethiolate] oxorhenium(V) ($^{186}$Re-MAG3-HBP), for the treatment of painful bone metastases. This agent showed a superior biodistribution as a bone-seeking agent in normal mice when compared with $^{186}$Re-1-hydroxyethylidene-1,1-diphosphonate ($^{186}$Re-HEDP). In this study, we evaluated the therapeutic effects of $^{186}$Re-MAG3-HBP using an animal model of bone metastasis. **Methods:** The model was prepared by injecting syngeneic MRMT-1 mammary tumor cells into the left tibia of female Sprague–Dawley rats. $^{186}$Re-MAG3-HBP (55.5, 111, or 222 MBq/kg) or $^{186}$Re-HEDP (55.5 MBq/kg) was then administered intravenously 21 d later. To evaluate the therapeutic effects and side effects, tumor size and peripheral blood cell counts were determined. Palliation of bone pain was evaluated by a von Frey filament test. **Results:** In the rats treated with $^{186}$Re-HEDP, tumor growth was comparable with that in untreated rats. In contrast, when $^{186}$Re-MAG3-HBP was administered, tumor growth was significantly inhibited. Allodynia induced by bone metastasis was attenuated by treatment with $^{186}$Re-MAG3-HBP or $^{186}$Re-HEDP, but $^{186}$Re-MAG3-HBP tended to be more effective. **Conclusion:** These results indicate that $^{186}$Re-MAG3-HBP could be useful as a therapeutic agent for the palliation of metastatic bone pain.

**Key Words:** bone metastases; internal radiotherapy; bisphosphonate; pain; radiopharmaceutical

**J Nucl Med 2007; 48:122–127**

Malignant tumors, especially cancers of the breast and prostate, frequently metastasize to bone (*1,2*). A prominent symptom of such metastasis is pain, which has a significant impact on patient quality of life, and pain within the skeletal tissues is the most common source of pain in patients with malignant disease (*3–5*). Treatments designed to reduce inflammation-associated pain with nonsteroidal antiinflammatory drugs (NSAIDs) are the first option in most cases, with stronger opioids used as the intensity of the pain rises. However, these drugs produce side effects such as gastrointestinal ulceration, neutropenia, enhanced bleeding, and deterioration of renal function in the case of NSAIDs, and nausea, sedation, and constipation in the case of opioids. Localized radiation therapy is an effective treatment for bone pain (*6*) but is difficult to apply when there are multiple lesion sites, as is often the case in patients with bone metastases. Wide-field, hemibody radiotherapy is also an effective treatment but its potential benefit is often outweighed by significant bone marrow and gastrointestinal toxicity. Accordingly, in cases of metastases to multiple sites, molecular radiotherapy using bone-seeking radiopharmaceuticals is preferable (*7,8*).

$^{186}$Re is a promising radionuclide with a maximum β-energy of 1.07 MeV and a γ-ray of 137 keV (9%) that are adequate for therapy and imaging, respectively. Furthermore, the physical half-life of $^{186}$Re is 3.8 d, which is long enough for shipment and processing of the radiopharmaceutical but not too long for its disposal as a radioactive waste. These physical characteristics have led to the development and clinical application of $^{186}$Re-1-hydroxyethylidene-1,1-diphosphonate ($^{186}$Re-HEDP) (*9,10*). However, $^{186}$Re-HEDP showed a delayed blood clearance and high gastric uptake after injection, due to its instability in vivo (*11–14*). Thus, to overcome the problems of $^{186}$Re-HEDP, we recently developed, based on the concept of bifunctional radiopharmaceuticals, a highly stable $^{186}$Re-mercaptoacetylglycylglycylglycylglycine (MAG3) complex–conjugated bisphosphonate, [[[[(4-hydroxy-4,4-diphosphonobutyl)carbamoylmethyl]carbamoylmethyl]carbamoylmethyl]carbamoylmethanethiolate] oxorhenium(V) ($^{186}$Re-MAG3-HBP, Fig. 1)

Received Jun. 26, 2006; revision accepted Sep. 25, 2006.

For correspondence or reprints contact: Hideo Saji, PhD, Department of Patho-Functional Bioanalysis, Graduate School of Pharmaceutical Sciences, Kyoto University, Sakyo-ku, Kyoto 606-8501, Japan.

E-mail: hsaji@pharm.kyoto-u.ac.jp

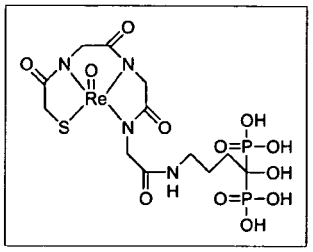

**FIGURE 1.** Chemical structure of Re-MAG3-HBP.

(*15*). This agent showed greater accumulation in bone and faster clearance from blood than $^{186}$Re-HEDP in normal mice.

In this study, we evaluated the therapeutic potential of $^{186}$Re-MAG3-HBP in comparison with $^{186}$Re-HEDP for the palliation of metastatic bone pain using an animal model of bone metastasis.

## MATERIALS AND METHODS

### Materials

$^{186}$Re was supplied by the Japan Atomic Energy Research Institute as perrhenate ($^{186}ReO_4^-$) at a specific activity of 18–20 TBq/g. Other reagents were of reagent grade and were used as received.

$^{186}$Re-HEDP, $^{186}$Re-MAG3-HBP, and nonradioactive Re-MAG3-HBP were prepared according to a published procedure (*15*) with radiochemical yields of >90% without requiring purification. The radiochemical purity of $^{186}$Re-HEDP was determined by thin-layer chromatography (TLC) and cellulose acetate electrophoresis (CAE) (Separax-SP; Joko Co. Ltd.). TLC analyses were performed with silica plates (Silica gel 60; Merck KGaA) with acetone as a developing solvent. $^{186}$Re-HEDP remained at the original position ($R_f$ = 0), whereas the free perrhenate ($^{186}ReO_4^-$) migrated with the solvent front ($R_f$ = 1). CAE was run at an electrostatic field of 0.8 mA/cm for 20 min in veronal buffer (ionic strength 0.06 M, pH 8.6). $^{186}$Re-HEDP migrated to the 3.5-cm anode from the origin, whereas reduced-hydrolyzed rhenium ($^{186}ReO_2$) remained at the origin. The radiochemical purity of $^{186}$Re-MAG3-HBP was determined by reversed-phase (RP) high-performance liquid chromatography (HPLC). RP-HPLC was performed with a Cosmosil 5$C_{18}$-AR-300 column (4.6 × 150 mm; Nacalai Tesque) at a flow rate of 1 mL/min with a mixture of 0.2 mol/L phosphate buffer (pH 6.0) and ethanol (90:10) containing 10 mmol/L tetrabutylammonium hydroxide.

### Biodistribution in Normal Rats

Experiments with animals were conducted in accordance with our institutional guidelines, and the experimental procedures were approved by the Kyoto University Animal Care Committee. Biodistribution experiments were performed by intravenously administering $^{186}$Re-labeled compounds into male Wistar rats (200–250 g). Groups of 4 rats each were administered 250 μL of each $^{186}$Re-labeled compound and sacrificed at 10 min, 3 h, and 24 h after injection. Tissues of interest were removed and weighed, and radioactivity counts were determined with an auto well γ-counter (ARC-2000; Aloka) and corrected for background radiation and physical decay during counting.

### Rat Model of Bone Metastasis

Female Sprague–Dawley rats were used (150–180 g). The animals were housed with free access to food and water at 25°C with a 12-h alternating light/dark cycle. MRMT-1 mammary tumor cells were kindly supplied by the Cell Resource Center for Biomedical Research, Tohoku University. The culture of MRMT-1 cells and induction of bone cancer was performed as previously described with slight modifications (*16*). Briefly, MRMT-1 cells were grown in cell culture dishes in RPMI 1640 medium with phenol red, 10% heat-inactivated fetal calf serum, 100 μg/mL glutamine, 100 units/mL penicillin, and 100 μg/mL streptomycin. The cells were cultured in a humidified atmosphere of 95% air and 5% carbon dioxide at 37°C. They were then released from the dishes by treatment with 0.05% trypsin/ethylenediaminetetraacetic acid. Next, the rats to be inoculated were anesthetized with chloral hydrate, and a 1.5-cm incision was made over the top half of the tibia. A 23-gauge needle was inserted into the intramedullary canal of the tibia, approximately 5 mm below the knee joint to create a cavity for injection of the cells. At the left tibia, 3 μL of medium with tumor cells (approximately $3 \times 10^3$ cells) was then injected into the bone cavity using a Hamilton syringe (Hamilton Co.). At the right tibia, 3 μL of medium only was injected into the bone cavity as a sham-treated control. The cavities were sealed using bone wax, and the wounds were closed with surgical suture.

### Imaging and Therapy

Rats were randomly distributed to the experimental groups. $^{186}$Re-MAG3-HBP (55.5, 111, or 222 MBq/kg), $^{186}$Re-HEDP (55.5 MBq/kg), or nonradioactive Re-MAG3-HBP was administered intravenously 21 d after inoculation—that is, the time needed for tumors to reach a palpable size (about 1 cm in diameter). A group of rats that did not receive any treatment served as a control group.

At 24 h after the injection of radiolabeled compounds, γ-imaging was performed on a SPECT-2000H (Hitachi Medical Co.) fitted with low-energy, high-resolution collimators. The energy window was symmetric (±20%) and centered on the $^{186}$Re photopeak (137 keV).

Tumoral bone-to-normal bone ratios were calculated by drawing regions of interest (ROIs) on planar images (counts/pixel). The ROI of tumoral bone was drawn manually around the edge of the tumoral bone activity by visual inspection. The ROI of normal bone was drawn at the corresponding site of the contralateral tibia (sham-treated) using an inverted figure of the tumoral bone ROI.

Tumor size was measured once weekly with a slide caliper in 2 dimensions. Individual tumor volumes (V) were calculated by the formula V = [length × (width)$^2$]/2 and related to the values on the day of treatment (relative tumor volume).

Pain was evaluated as the hind paw withdrawal response to stimulation with von Frey filaments (North Coast Medical) as previously described with slight modifications (*17,18*). The test environment consisted of a wire mesh box. The rat was placed in the test box and allowed to acclimate for 5–10 min. The tactile stimulus was applied to the plantar surface in ascending order of force beginning with the 2.84-mN filament. Once a withdrawal response was established, the paw was retested, starting with the next descending von Frey filament until no response occurred. The lowest amount of force required to elicit a response was recorded as the paw withdrawal threshold (in newtons [N]). The ratio of the right value to the left value was used as an index of the palliation of pain.

The myelotoxicity of the radiotherapy was assessed using the peripheral blood cell counts. Two blood samples (5 μL) were obtained from a tail vein. The samples were pooled and diluted with 95 μL of Turk's solution (0.01% gentian violet and 1% acetic acid) for white blood cell (WBC) counts and 495 μL of 1% ammonium oxalate for platelet counts, and cell counts were performed using a hemocytometer and a light microscope.

### Statistical Evaluation

An unpaired Student $t$ test was used for the biodistribution experiments. One-way ANOVA followed by the Dunnett post hoc test compared with the untreated group was used for experiments on allodynia measurements, comparisons of tumor growth, WBC counts, and platelet counts. Results were considered statistically significant at $P < 0.05$.

## RESULTS

### Biodistribution in Normal Rats

The biodistributions of $^{186}$Re-MAG3-HBP and $^{186}$Re-HEDP in normal rats are presented in Table 1. Both compounds showed a rapid accumulation and long residence in the bone. The uptake of $^{186}$Re-MAG3-HBP in the bone was significantly higher than that of $^{186}$Re-HEDP.

### Imaging

The planar images at 24 h after injection of $^{186}$Re-MAG3-HBP and $^{186}$Re-HEDP showed a marked accumulation of radioactivity surrounding the site of inoculation of the tumor cells (Fig. 2). In tissues other than bone, no significant accumulation of radioactivity was observed, a reflection of the results of the biodistribution experiments.

Tumoral bone-to-normal bone ratios of $^{186}$Re-MAG3-HBP and $^{186}$Re-HEDP were 3.54 ± 0.60 and 2.90 ± 0.97, respectively (mean ± SD). This difference was not statistically significant.

**TABLE 1**
Biodistribution of $^{186}$Re-MAG3-HBP and $^{186}$Re-HEDP in Rats

| Tissue | Time after administration | | |
|---|---|---|---|
| | 10 min | 3 h | 24 h |
| | $^{186}$Re-MAG3-HBP (%ID/g tissue) | | |
| Blood | 0.831 ± 0.134* | 0.015 ± 0.008† | 0.003 ± 0.000† |
| Liver | 0.213 ± 0.031* | 0.063 ± 0.025 | 0.051 ± 0.009† |
| Kidney | 1.551 ± 0.115 | 0.539 ± 0.187* | 0.473 ± 0.074 |
| Intestine | 0.153 ± 0.015* | 0.235 ± 0.173 | 0.151 ± 0.081 |
| Spleen | 0.180 ± 0.018* | 0.030 ± 0.009 | 0.027 ± 0.005* |
| Pancreas | 0.196 ± 0.024 | 0.013 ± 0.003* | 0.008 ± 0.002 |
| Lung | 0.566 ± 0.059† | 0.040 ± 0.009* | 0.037 ± 0.031 |
| Stomach‡ | 0.525 ± 0.198 | 0.302 ± 0.134* | 0.152 ± 0.176* |
| Femur | 2.129 ± 0.142* | 3.943 ± 0.270† | 4.097 ± 0.181† |
| Muscle | 0.129 ± 0.028 | 0.014 ± 0.009 | 0.004 ± 0.001 |
| | $^{186}$Re-HEDP (%ID/g tissue) | | |
| Blood | 0.572 ± 0.103 | 0.074 ± 0.025 | 0.025 ± 0.006 |
| Liver | 0.162 ± 0.020 | 0.035 ± 0.005 | 0.025 ± 0.005 |
| Kidney | 1.807 ± 0.613 | 0.859 ± 0.162 | 0.386 ± 0.115 |
| Intestine | 0.126 ± 0.012 | 0.074 ± 0.039 | 0.082 ± 0.039 |
| Spleen | 0.133 ± 0.019 | 0.032 ± 0.005 | 0.020 ± 0.003 |
| Pancreas | 0.164 ± 0.021 | 0.019 ± 0.003 | 0.013 ± 0.004 |
| Lung | 0.414 ± 0.049 | 0.067 ± 0.014 | 0.032 ± 0.013 |
| Stomach‡ | 0.710 ± 0.323 | 0.729 ± 0.284 | 0.764 ± 0.440 |
| Femur | 1.586 ± 0.365 | 1.913 ± 0.272 | 1.798 ± 0.621 |
| Muscle | 0.117 ± 0.024 | 0.011 ± 0.005 | 0.005 ± 0.003 |

*$P < 0.05$ vs. $^{186}$Re-HEDP.
†$P < 0.01$ vs. $^{186}$Re-HEDP.
‡Data are expressed as percentage injected dose (%ID).
Data are expressed as mean ± SD for 4 animals.

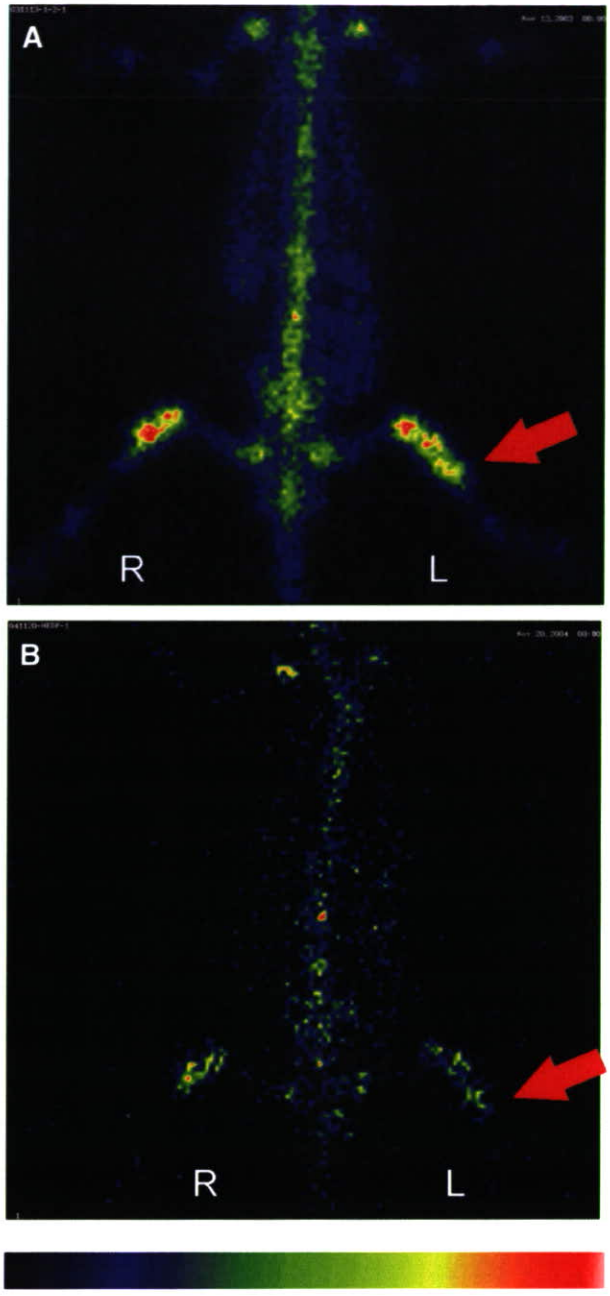


**FIGURE 2.** Planar images at 24 h after intravenous injection of $^{186}$Re-MAG3-HBP (222 MBq/kg) (A) and $^{186}$Re-HEDP (55.5 MBq/kg) (B). Arrows indicate the site where tumor cells were injected.

### Therapeutic Effects

The volume of the tumors as a function of time is shown in Figure 3. As can be seen, the MRMT-1 tumor cells proliferated exponentially after a palpable tumor developed in the left tibia. In rats treated with $^{186}$Re-HEDP at a dose of 55.5 MBq/kg, tumor growth was comparable with that of untreated rats. In

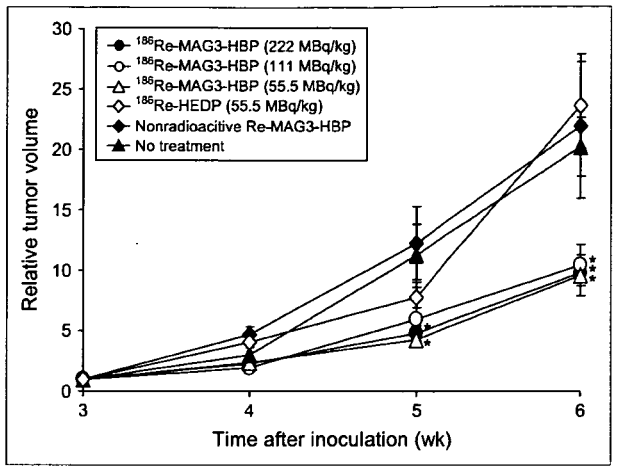


**FIGURE 3.** Curves show inhibition of growth of MRMT-1 tumor cells on therapy. Data are expressed as tumor volume relative to that on day of treatment (mean ± SEM for 5–7 rats). Significance was determined using 1-way ANOVA followed by the Dunnett post hoc test (*$P < 0.05$ vs. no treatment).

contrast, when $^{186}$Re-MAG3-HBP was administered at the same dose as $^{186}$Re-HEDP, tumor growth was significantly inhibited compared with that of the untreated group.

Palliative effects determined by the von Frey filament test are shown in Figure 4. A larger value indicates more intense pain on the cancer-bearing side. In untreated rats, the enhanced withdrawal response to mechanical stimulation with von Frey filaments caused by cancer-induced bone pain was elevated. Both $^{186}$Re-MAG3-HBP and $^{186}$Re-HEDP attenuated this mechanical allodynia but $^{186}$Re-MAG3-HBP tended to be more effective.

The injected dose of $^{186}$Re-MAG3-HBP ranged from 55.5 to 222 MBq/kg, and the therapeutic effects were assessed. Consequently, it was found that the inhibition of tumor growth and the response in terms of the palliation of pain were not correlated with the treatment dose (Figs. 3 and 4).

Moreover, when nonradioactive Re-MAG3-HBP was administered, tumor growth and the withdrawal response were not significant compared with those in untreated rats (Figs. 3 and 4).

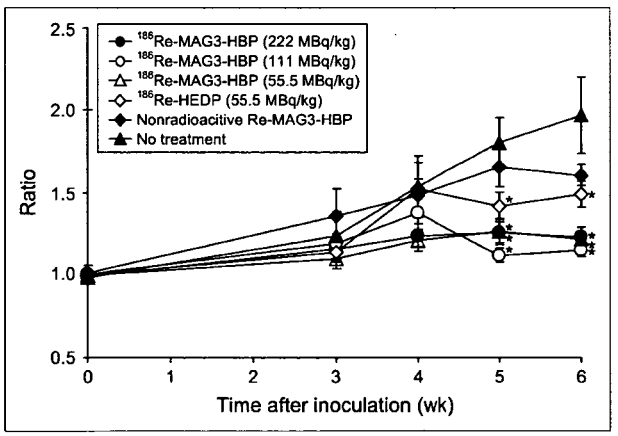


**FIGURE 4.** Effects of radiopharmaceuticals on bone cancer pain. Data are expressed as ratio of right (contralateral) withdrawal paw threshold values to left (ipsilateral) values (mean ± SEM for 5–7 rats). Significance was determined using 1-way ANOVA followed by the Dunnett post hoc test (*$P < 0.05$ vs. no treatment).

### Myelotoxicity

When $^{186}$Re-MAG3-HBP or $^{186}$Re-HEDP was administered, WBC and platelet counts tended to decrease at 1 and 2 wk after treatment, especially in the case of high-dose treatment with $^{186}$Re-MAG3-HBP. However, the decreases were not critical, and these counts were recovered within 3 wk after the injection (Fig. 5).

## DISCUSSION

In general, the use of an appropriate animal model is important for the evaluation of the therapeutic effects of

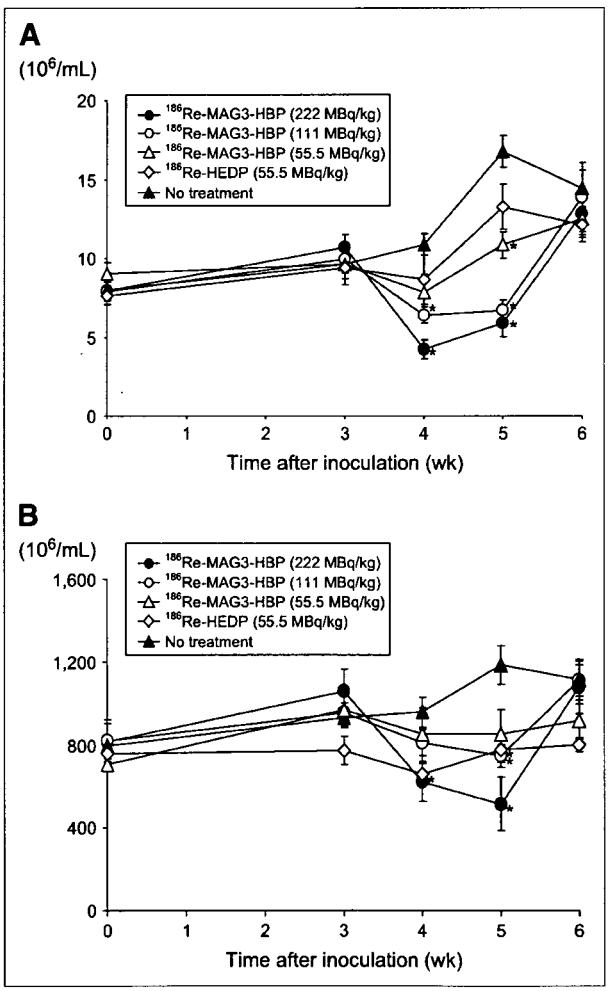


**FIGURE 5.** WBC (A) and thrombocyte (B) counts in rat model of bone metastasis under treatment. Data are presented as mean ± SEM for 5–7 rats. Significance was determined using 1-way ANOVA followed by the Dunnett post hoc test (*$P < 0.05$ vs. no treatment).

pharmaceuticals. For the evaluation of therapeutic effects of radiopharmaceuticals on metastatic bone tumors, a heart injection model has often been used (*19,20*). This model involves the direct introduction of tumor cells into the arterial circulation through the left ventricle of the heart in nude mice or nude rats (*21,22*). It is useful for the evaluation of survival (*19,20*) but is unsuitable for the evaluation of palliation of metastatic bone pain because it has multiple lesion sites. Furthermore, to our knowledge, there has been no report on an appropriate animal model for the evaluation of the palliating effects of radiopharmaceuticals on metastatic bone pain. However, intrabone injection models have recently been developed as a model of bone tumor pain (*16,23,24*). In this study, we used one of these models, the intratibial injection model, for the following reasons: (a) the radiologic, histologic, and behavioral characteristics resemble those of patients with bone metastases (*5,16,25*); (b) it is possible to equalize the position of single lesions in all experimental animals; (c) bone cancer pain can be quantitatively evaluated using a von Frey filament test; and (d) the surgery is simple and barely invasive.

The von Frey filament test is a way to examine withdrawal responses for mechanical stimuli to the hind paw of rats using various different von Frey filaments and has frequently been used for evaluating mechanical allodynia, especially in a neuropathic pain model (*17,18*). Recently, the test has also been used in a metastasis model (*16,25*). Bone cancer pain can be intermittent, but it progresses rapidly into continuous pain that is exacerbated by episodes of breakthrough pain. Once this chronic pain is established, the condition of the patient deteriorates further when mechanical allodynia develops. Mechanical allodynia occurs when normally nonpainful activity or stimulation is perceived as painful. For example, coughing, turning in bed, or gentle limb movement can cause intense pain (*26*). Accordingly, evaluating mechanical allodynia as an index of pain in the model is meaningful.

Moreover, it has been reported that levels of osteoblastic/osteoclastic activity were high in areas close to the tumor because the MRMT-1 cells used in this model produce a mixed type of bone lesion (*16*). Most bone-seeking radiopharmaceuticals, including $^{186}$Re-MAG3-HBP, accumulate at sites with strong osteoblastic activity. Accordingly, we assumed that this model might be adequate to evaluate the therapeutic effects of bone-seeking radiopharmaceuticals.

The main finding of this study is that a single treatment with $^{186}$Re-MAG3-HBP, a $^{186}$Re-complex–conjugated bisphosphonate, achieved significant inhibition of tumor growth and palliation of pain in a rat model of bone metastasis (Figs. 3 and 4). $^{186}$Re-HEDP palliated the pain but did not inhibit tumor growth. Although the mechanism of the palliation of bone cancer pain by radiotherapy remains unclear, a radiation-induced reduction of tumor size has been considered one of the causes (*27,28*). However, empiric data from experiments with external irradiation indicate that the absorbed dose required to achieve pain relief is significantly lower than that necessary to achieve a tumoricidal effect (*29–31*). Because $^{186}$Re-MAG3-HBP showed much greater accumulation in normal bone than did $^{186}$Re-HEDP in biodistribution experiments with normal rats and because there was no significant difference between the tumoral bone-to-normal bone ratios of $^{186}$Re-MAG3-HBP and $^{186}$Re-HEDP in the bone metastasis model, the difference in the inhibition of tumor growth between the 2 radiopharmaceuticals could be attributed to the difference in accumulation at the site of bone metastasis. Furthermore, the inhibition of tumor growth should result in a more effective palliation than that achieved with $^{186}$Re-HEDP.

The pain-relieving effect of $^{186}$Re-MAG3-HBP was not dependent on dose (Fig. 4). This result is consistent with the clinical observations in breast cancer patients that the response rate in terms of pain reduction was not correlated with the dose of $^{186}$Re-HEDP (*10*). Contrary to expectation, raising the dose of $^{186}$Re-MAG3-HBP did not potentiate the inhibition of tumor growth. Although the reason for this is unclear, no serious toxic effects were observed on high-dose treatment. Therefore, it is necessary to examine the effect of increasing the dose of $^{186}$Re-MAG3-HBP on tumor growth using other models.

Bisphosphonates have been used primarily to treat hypercalcemia (from excess bone resorption) and, more recently, cancer-induced bone pain (*32*). Recent reports indicate that the regular use of bisphosphonates for metastatic bone disease prevents skeletal-related events, reduces bone pain, and improves the patient's quality of life (*32,33*). Briefly, the mechanism of action includes induction of the apoptosis of osteoclasts, inhibition of the proliferation of cancer cells, and reduction in the production of cytokine and secretion of metalloproteinase. Walker et al. reported that zoledronic acid, a bisphosphonate, was a useful antinociceptive agent in a rat model of metastatic cancer pain (*25*). These findings raise the possibility that the therapeutic effect of $^{186}$Re-MAG3-HBP is attributable not to the β-particles of $^{186}$Re but, rather, to the bisphosphonate structure of $^{186}$Re-MAG3-HBP. To test this possibility, we treated rats with nonradioactive Re-MAG3-HBP at the same dose as $^{186}$Re-MAG3-HBP. In nonradioactive Re-MAG3-HBP–treated rats, tumor growth and the withdrawal response were comparable with those in untreated rats (Figs. 3 and 4). Accordingly, the therapeutic effect of $^{186}$Re-MAG3-HBP can be attributed to the β-particles of $^{186}$Re.

## CONCLUSION

$^{186}$Re-MAG3-HBP accumulated at the site where tumor cells were injected in a rat model of bone cancer and significantly inhibited tumor growth and attenuated the allodynia induced by bone cancer without having critical myelosuppressive side effects. These results indicate that $^{186}$Re-MAG3-HBP could be useful as a therapeutic agent for the palliation of metastatic bone pain.

## ACKNOWLEDGMENTS

This work was supported in part by a Grant-in-Aid for Scientific Research on Priority Areas from the Ministry of

Education, Culture, Sports, Science and Technology of Japan and by a research grant from the Sagawa Foundation for the Promotion of Cancer Research.

## REFERENCES


1. Yoneda T, Sasaki A, Mundy GR. Osteolytic bone metastasis in breast cancer. *Breast Cancer Res Treat.* 1994;32:73–84.
2. Coleman RE. Skeletal complications of malignancy. *Cancer.* 1997;80:1588–1594.
3. Portenoy RK, Lesage P. Management of cancer pain. *Lancet.* 1999;353:1695–1700.
4. Portenoy RK, Payne D, Jacobsen P. Breakthrough pain: characteristics and impact in patients with cancer pain. *Pain.* 1999;81:129–134.
5. Mercadante S. Malignant bone pain: pathophysiology and treatment. *Pain.* 1997; 69:1–18.
6. Arcangeli G, Giovinazzo G, Saracino B, D'Angelo L, Giannarelli D, Micheli A. Radiation therapy in the management of symptomatic bone metastases: the effect of total dose and histology on pain relief and response duration. *Int J Radiat Oncol Biol Phys.* 1998;42:1119–1126.
7. Lewington VJ. Bone-seeking radionuclides for therapy. *J Nucl Med.* 2005; 46(suppl 1):38S–47S.
8. Finlay IG, Mason MD, Shelley M. Radioisotopes for the palliation of metastatic bone cancer: a systematic review. *Lancet Oncol.* 2005;6:392–400.
9. Limouris GS, Shukla SK, Condi-Paphiti A, et al. Palliative therapy using rhenium-186-HEDP in painful breast osseous metastases. *Anticancer Res.* 1997; 17:1767–1772.
10. Lam MG, de Klerk JM, van Rijk PP. $^{186}$Re-HEDP for metastatic bone pain in breast cancer patients. *Eur J Nucl Med Mol Imaging.* 2004;31(suppl 1):S162–S170.
11. de Klerk JM, van Dijk A, van het Schip AD, Zonnenberg BA, van Rijk PP. Pharmacokinetics of rhenium-186 after administration of rhenium-186-HEDP to patients with bone metastases. *J Nucl Med.* 1992;33:646–651.
12. De Winter F, Brans B, Van De Wiele C, Dierckx RA. Visualization of the stomach on rhenium-186 HEDP imaging after therapy for metastasized prostate carcinoma. *Clin Nucl Med.* 1999;24:898–899.
13. Ogawa K, Mukai T, Arano Y, et al. Design of a radiopharmaceutical for the palliation of painful bone metastases: rhenium-186-labeled bisphosphonate derivative. *J Labelled Compds Radiopharm.* 2004;47:753–761.
14. Ogawa K, Mukai T, Arano Y, et al. Rhemium-186-monoaminemonoamidedithiols conjugated bisphosphonate derivatives for bone pain palliation. *Nucl Med Biol.* 2006;33:513–520.
15. Ogawa K, Mukai T, Arano Y, et al. Development of a rhenium-186-labeled MAG3-conjugated bisphosphonate for the palliation of metastatic bone pain based on the concept of bifunctional radiopharmaceuticals. *Bioconjug Chem.* 2005;16:751–757.
16. Medhurst SJ, Walker K, Bowes M, et al. A rat model of bone cancer pain. *Pain.* 2002;96:129–140.
17. Kim SH, Chung JM. An experimental model for peripheral neuropathy produced by segmental spinal nerve ligation in the rat. *Pain.* 1992;50:355–363.
18. Okada M, Nakagawa T, Minami M, Satoh M. Analgesic effects of intrathecal administration of P2Y nucleotide receptor agonists UTP and UDP in normal and neuropathic pain model rats. *J Pharmacol Exp Ther.* 2002;303:66–73.
19. Henriksen G, Breistol K, Bruland O, Fodstad O, Larsen R. Significant antitumor effect from bone-seeking, alpha-particle-emitting $^{223}$Ra demonstrated in an experimental skeletal metastases model. *Cancer Res.* 2002;62:3120–3125.
20. Arstad E, Hoff P, Skattebol L, Skretting A, Breistol K. Studies on the synthesis and biological properties of non-carrier-added [$^{125}$I and $^{131}$I]-labeled arylalkylidenebisphosphonates: potent bone-seekers for diagnosis and therapy of malignant osseous lesions. *J Med Chem.* 2003;46:3021–3032.
21. Engebraaten O, Fodstad O. Site-specific experimental metastasis patterns of two human breast cancer cell lines in nude rats. *Int J Cancer.* 1999;82:219–225.
22. Yoneda T, Michigami T, Yi B, Williams PJ, Niewolna M, Hiraga T. Actions of bisphosphonate on bone metastasis in animal models of breast carcinoma. *Cancer.* 2000;88:2979–2988.
23. Schwei MJ, Honore P, Rogers SD, et al. Neurochemical and cellular reorganization of the spinal cord in a murine model of bone cancer pain. *J Neurosci.* 1999;19:10886–10897.
24. Honore P, Luger NM, Sabino MA, et al. Osteoprotegerin blocks bone cancer-induced skeletal destruction, skeletal pain and pain-related neurochemical reorganization of the spinal cord. *Nat Med.* 2000;6:521–528.
25. Walker K, Medhurst SJ, Kidd BL, et al. Disease modifying and anti-nociceptive effects of the bisphosphonate, zoledronic acid in a model of bone cancer pain. *Pain.* 2002;100:219–229.
26. Clohisy DR, Mantyh PW. Bone cancer pain. *Cancer.* 2003;97:866–873.
27. Goblirsch M, Mathews W, Lynch C, et al. Radiation treatment decreases bone cancer pain, osteolysis and tumor size. *Radiat Res.* 2004;161:228–234.
28. Bone Pain Trial Working Party. 8 Gy single fraction radiotherapy for the treatment of metastatic skeletal pain: randomised comparison with a multifraction schedule over 12 months of patient follow-up. *Radiother Oncol.* 1999;52:111–121.
29. Hoskin PJ. Bisphosphonates and radiation therapy for palliation of metastatic bone disease. *Cancer Treat Rev.* 2003;29:321–327.
30. Vakaet LA, Boterberg T. Pain control by ionizing radiation of bone metastasis. *Int J Dev Biol.* 2004;48:599–606.
31. Vit JP, Ohara PT, Tien DA, et al. The analgesic effect of low dose focal irradiation in a mouse model of bone cancer is associated with spinal changes in neuro-mediators of nociception. *Pain.* 2006;120:188–201.
32. Mystakidou K, Katsouda E, Stathopoulou E, Vlahos L. Approaches to managing bone metastases from breast cancer: the role of bisphosphonates. *Cancer Treat Rev.* 2005;31:303–311.
33. Body JJ. Bisphosphonates for malignancy-related bone disease: current status, future developments. *Support Care Cancer.* 2006;14:408–418.

# Development of a Novel $^{99m}$Tc-Chelate–Conjugated Bisphosphonate with High Affinity for Bone as a Bone Scintigraphic Agent

Kazuma Ogawa[1,2], Takahiro Mukai[1,3], Yasuyuki Inoue[1], Masahiro Ono[1], and Hideo Saji[1]

*[1]Department of Patho-Functional Bioanalysis, Graduate School of Pharmaceutical Sciences, Kyoto University, Kyoto, Japan; [2]Division of Tracer Kinetics, Advanced Science Research Center, Kanazawa University, Kanazawa, Japan; and [3]Department of Biomolecular Recognition Chemistry, Graduate School of Pharmaceutical Sciences, Kyushu University, Fukuoka, Japan*

In bone scintigraphy using $^{99m}$Tc with methylenediphosphonate ($^{99m}$Tc-MDP) and hydroxymethylenediphosphonate ($^{99m}$Tc-HMDP), it takes 2–6 h after an injection before imaging can start. This interval could be shortened with a new radiopharmaceutical with higher affinity for bone. Here, based on the concept of bifunctional radiopharmaceuticals, we designed a $^{99m}$Tc-mercaptoacetylglycylglycylglycine (MAG3)-conjugated hydroxy-bisphosphonate (HBP) ($^{99m}$Tc-MAG3-HBP) and a $^{99m}$Tc-6-hydrazinopyridine-3-carboxylic acid (HYNIC)-conjugated hydroxy-bisphosphonate ($^{99m}$Tc-HYNIC-HBP). **Methods:** $^{99m}$Tc-MAG3-HBP was prepared by complexation of MAG3-HBP with $^{99m}$Tc using $SnCl_2$ as a reductant. The precursor of $^{99m}$Tc-HYNIC-HBP, HYNIC-HBP, was obtained by deprotection of the Boc group after the coupling of Boc-HYNIC to a bisphosphonate derivative. $^{99m}$Tc-HYNIC-HBP was prepared by a 1-pot reaction of HYNIC-HBP with $^{99m}TcO_4^-$, tricine, and 3-acetylpyridine in the presence of $SnCl_2$. Affinity for bone was evaluated in vitro by hydroxyapatite-binding assays for $^{99m}$Tc-HMDP, $^{99m}$Tc-MAG3-HBP, and $^{99m}$Tc-HYNIC-HBP. Biodistribution experiments for the 3 $^{99m}$Tc-labeled compounds were performed on normal rats. **Results:** $^{99m}$Tc-MAG3-HBP and $^{99m}$Tc-HYNIC-HBP were each prepared with a radiochemical purity of >95%. In the in vitro binding assay, $^{99m}$Tc-MAG3-HBP and $^{99m}$Tc-HYNIC-HBP had greater affinity for hydroxyapatite than $^{99m}$Tc-HMDP. In the biodistribution experiments, $^{99m}$Tc-MAG3-HBP and $^{99m}$Tc-HYNIC-HBP had higher levels of radioactivity in bone than $^{99m}$Tc-HMDP. $^{99m}$Tc-MAG3-HBP was cleared from the blood slower than $^{99m}$Tc-HMDP, whereas there was no significant difference in clearance between $^{99m}$Tc-HYNIC-HBP and $^{99m}$Tc-HMDP. Consequently, $^{99m}$Tc-HYNIC-HBP showed a higher bone-to-blood ratio than $^{99m}$Tc-HMDP. **Conclusion:** We developed a novel $^{99m}$Tc-chelate–conjugated bisphosphonate with high affinity for bone and rapid clearance from blood, based on the concept of bifunctional radiopharmaceuticals. The present findings indicate that $^{99m}$Tc-HYNIC-HBP holds great potential for bone scintigraphy.

**Key Words:** bone scintigraphy; bisphosphonate; $^{99m}$Tc; MAG3; HYNIC

**J Nucl Med 2006; 47:2042–2047**

Over the last quarter of a century, complexes of $^{99m}$Tc with methylenediphosphonate ($^{99m}$Tc-MDP) and hydroxymethylenediphosphonate ($^{99m}$Tc-HMDP) have been widely used as radiopharmaceuticals for bone scintigraphy in cases of metastatic bone disease, Paget's disease, fractures in osteoporosis, and so forth (*1–4*). With these $^{99m}$Tc-labeled bisphosphonates, however, an interval of 2–6 h is needed between injection and bone imaging (*3*). Shorting this interval would lessen the burden on patients in terms of the total length of the examination and the dose of radiation absorbed. To enable imaging at an earlier time after injection, a radiopharmaceutical with higher affinity for bone is required.

Bisphosphonate analogs accumulate in bone because their phosphonate groups bind to the $Ca^{2+}$ of hydroxyapatite crystals (*5*). In the case of $^{99m}$Tc-MDP and $^{99m}$Tc-HMDP, the phosphonate groups coordinate with technetium (*6*), which might decrease the inherent accumulation of MDP and HMDP in bone. Thus, we hypothesized that bone affinity of $^{99m}$Tc-labeled bisphosphonate would be increased by the design of a bisphosphonate in which the phosphonate groups do not coordinate with technetium, and we attempted to design a $^{99m}$Tc-chelate–conjugated bisphosphonate based on the concept of bifunctional radiopharmaceuticals (Fig. 1). In this study, mercaptoacetylglycylglycylglycine (MAG3) and 6-hydrazinopyridine-3-carboxylic acid (HYNIC) were chosen as chelating sites because they have been widely used for $^{99m}$Tc labeling of proteins and peptides (*7–11*) and conjugated to 4-amino-1-hydroxybutylidene-1,1-bisphosphonate. Then, $^{99m}$Tc-[[[(4-hydroxy-4,4-diphosphonobutyl)carbamoylmethyl]carbamoylmethyl]carbamoylmethyl]carbamoylmethanethiolate ($^{99m}$Tc-MAG3-HBP; Fig. 1A) and [$^{99m}$Tc][[4-[(6-hydrazinopyridine-3-carbonyl)amino]-1-hydroxy-1-phosphonobutyl]phosphonic acid](tricine)(3-acetylpyridine) ($^{99m}$Tc-HYNIC-HBP; Fig. 1B) were

Received May 9, 2006; Revision accepted Sep. 6, 2006.

For correspondence or reprints contact: Hideo Saji, PhD, Department of Patho-Functional Bioanalysis, Graduate School of Pharmaceutical Sciences, Kyoto University, Sakyo-ku, Kyoto 606-8501, Japan.

E-mail: hsaji@pharm.kyoto-u.ac.jp

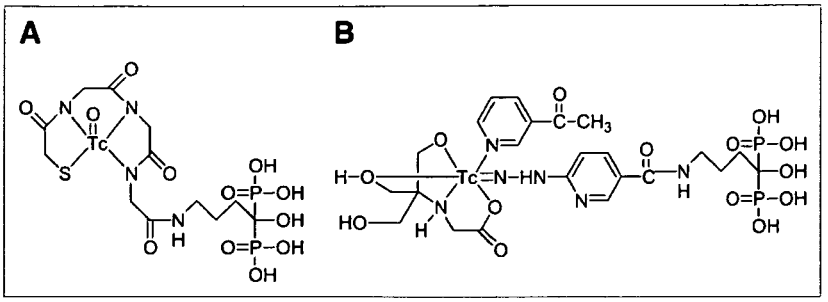


**FIGURE 1.** Chemical structures of $^{99m}$Tc-MAG3-HBP (A) and $^{99m}$Tc-HYNIC-HBP (B).

prepared by coordination with $^{99m}$Tc, and their properties in vitro and in vivo were compared with these of $^{99m}$Tc-HMDP.

## MATERIALS AND METHODS

### Materials

Proton nuclear magnetic resonance ($^1$H NMR) spectra were recorded on a Bruker AC-200 spectrometer (JEOL Ltd.), and the chemical shifts were reported in parts per million downfield from an internal 3-(trimethylsilyl)propionic-2,2,3,3-$d_4$ acid sodium salt standard. Electrospray ionization mass spectra (ESI-MS) were obtained with a LCMS-QP8000α (Shimadzu). Thin-layer chromatographic analyses were performed with silica plates (Silica gel 60; Merck KGaA) with acetone as a developing solvent. $^{99m}$Tc-Pertechnetate ($^{99m}TcO_4^-$) was eluted in a saline solution on a daily basis from generators (Daiichi Radioisotope Laboratories, Ltd.). $^{99m}$Tc-HMDP was prepared by reconstitution with a conventional HMDP labeling kit (Nihon Medi-Physics Co., Ltd.) with a $^{99m}TcO_4^-$ solution. Other reagents were of reagent grade and were used as received.

### Preparation of $^{99m}$Tc-MAG3-HBP

The precursor of $^{99m}$Tc-MAG3-HBP, [1-hydroxy-1-phosphono-4-[2-[2-[2-(2-tritylmercaptoacetylamino)-acetylamino]acetylamino] acetylamino]butyl]phosphonic acid (Tr-MAG3-HBP) was synthesized according to procedures described previously (*12*). The trityl group of Tr-MAG3-HBP (0.1 mg) was dissolved in 190 μL of trifluoroacetic acid (TFA) and 10 μL of triethylsilane. After removal of the solvent under a stream of $N_2$, 80 μL of 0.1 mol/L borate buffer (pH 9.5) were added to the residue. Next, 3 μL of $SnCl_2 \cdot 2H_2O$ solution in 0.1 mol/L citrate buffer (pH 5.0) (1 mg/mL) and 200 μL of $^{99m}TcO_4^-$ solution were added, and the reaction mixture was vigorously stirred and allowed to react at 95°C for 1 h. $^{99m}$Tc-MAG3-HBP was purified by reversed-phase high-performance liquid chromatography (RP-HPLC) performed with a Cosmosil 5$C_{18}$-AR-300 column (4.6 × 150 mm; Nacalai Tesque) at a flow rate of 1 mL/min with a mixture of 0.2 mol/L phosphate buffer (pH 6.0) and ethanol (90:10) containing 10 mmol/L tetrabutylammonium hydroxide.

### Preparation of [[[[(4-Hydroxy-4,4-Diphosphonobutyl) Carbamoylmethyl]Carbamoylmethyl]Carbamoylmethyl] Carbamoylmethanethiolate] Oxorhenium(V) (Re-MAG3-HBP)

Re-MAG3-HBP was synthesized according to procedures described previously (*12*). ESI-MS calculated for $C_{12}H_{20}N_4O_{12}P_2{}^{187}ReS$ (M- H)$^-$: m/z 692. Found: 692 $C_{12}H_{20}N_4O_{12}P_2{}^{185}ReS$ (M- H)$^-$: m/z 690. Found: 690.

### Preparation of $^{99m}$Tc-HYNIC-HBP

2,3,5,6-Tetrafluorophenyl 6-(tert-butoxycarbonyl)-hydrazinopyridine-3-carboxylate (Boc-HYNIC-TFP) and 4-amino-1-hydroxybutylidene-1,1-bisphosphonate were synthesized according to procedures described preciously (*12,13*). 4-Amino-1-hydroxybutylidene-1,1-bisphosphonate (10.3 mg, 41.3 μmol) was suspended in 1.33 mL of distilled water, and triethylamine (25.1 mg, 248 μmol) was added to the suspension. After a few seconds of stirring at room temperature, Boc-HYNIC-TFP (17.8 mg, 44.4 μmol) dissolved in 1.33 mL of acetonitrile was added. The reaction mixture was stirred for 3 h at room temperature. RP-HPLC was performed with a Hydrosphere 5C18 column (20 × 150 mm; YMC Co., Ltd) at a flow rate of 16 mL/min with a mixture of water, acetonitrile, and formic acid (90:10:1). Chromatograms were obtained by monitoring the ultraviolet (UV) adsorption at a wavelength of 254 nm. The fraction containing [4-[[6-(tert-butoxycarbonyl)-hydrazinopyridine-3-carbonyl]amino]-1-hydroxy-1-phosphonobutyl]phosphonic acid (Boc-HYNIC-HBP) was identified by mass spectrometry and collected. The solvent was removed by lyophilization to provide Boc-HYNIC-HBP (178 mg, 36.7%) as white crystals. $^1$H NMR ($D_2O$): δ 8.42 (1H, s), 8.33 (1H, d), 7.21 (1H, d), 3.43 (2H, t), 1.92−2.04 (4H, m), 1.47 (9H, s). ESI-MS calculated for $C_{15}H_{26}N_4O_{10}P_2$ (M- H)$^-$: m/z 483. Found: 483.

Boc-HYNIC-HBP (10.4 mg, 21.5 μmol) was stirred in a mixed solution of TFA (720 μL) and anisole (80 μL) for 10 min at room temperature. After removal of the solvent under a stream of $N_2$, the residue was washed with dry ether to produce [4-[(6-hydrazinopyridine-3-carbonyl)amino]-1-hydroxy-1-phosphonobutyl]phosphonic acid (HYNIC-HBP) quantitatively as white crystals. $^1$H NMR ($D_2O$): δ 8.33 (1H, s), 8.13 (1H, d), 7.01 (1H, d), 3.42 (2H, t), 1.94−2.04 (4H, m). ESI-MS calculated for $C_{10}H_{18}N_4O_8P_2$ (M- H)$^-$: m/z 383. Found: 383.

Forty microliters of HYNIC-HBP solution (3.75 mg/mL in 0.1 mol/L borate buffer, pH 9.5) were mixed successively with 200 μL of tricine solution (30 mg/mL in 10 mmol/L citrate buffer, pH 5.2), 200 μL of 3-acetylpyridine solution (10 μL/mL in 10 mmol/L citrate buffer, pH 5.2), 200 μL of $^{99m}TcO_4^-$ solution, and 25 μL of $SnCl_2$ solution (1.0 mg/mL in 0.1N HCl). The reaction mixture was vigorously stirred and allowed to react at 95°C for 35 min. $^{99m}$Tc-HYNIC-HBP was purified by RP-HPLC under the same conditions as for the preparation of $^{99m}$Tc-MAG3-HBP.

### Hydroxyapatite-Binding Assay

The hydroxyapatite-binding assay was performed according to procedures described preciously with a slight modification (*14–16*). In brief, hydroxyapatite beads (Bio-Gel; Bio-Rad) were suspended in Tris/HCl-buffered saline (50 mmol/L, pH 7.4) at 1,

2.5, and 10 mg/mL. For the solutions of $^{99m}$Tc-labeled compounds ($^{99m}$Tc-MAG3-HBP, $^{99m}$Tc-HYNIC-HBP, and $^{99m}$Tc-HMDP), the bisphosphonate concentrations were adjusted to 0.60 μmol/L. One hundred microliters of each solution of $^{99m}$Tc-labeled compound were added to 100 μL of the hydroxyapatite suspension, and samples were gently shaken for 1 h at room temperature because it has been reported that 1 h was enough to attain binding equilibrium (*14*). After centrifugation at 10,000*g* for 5 min, the radioactivity of the supernatant was measured with an auto well γ-counter (ARC-2000; Aloka). Control experiments were performed with a similar procedure in the absence of hydroxyapatite beads. The rate of binding was determined as follows:

Hydroxyapatite binding (%) = (1 − [radioactivity of supernatant of each sample]/[radioactivity of supernatant in the respective control]) × 100.

### Biodistribution Experiments

Animal experiments were conducted in accordance with our institutional guidelines, and the experimental procedures were approved by the Kyoto University Animal Care Committee. Biodistribution experiments were performed with an intravenous administration of 250 μL of each diluted tracer solution (370–740 kBq) to male Wistar rats (200–230 g). Groups of at least 4 rats each were sacrificed by decapitation at 5, 10, 30, and 60 min after injection. Organs of interest were removed and weighed, and radioactivity counts were determined with an auto well γ-counter and corrected for background radiation and physical decay during counting.

### Serum Protein-Binding Assay

The binding of $^{99m}$Tc-labeled compounds to serum protein was evaluated by ultrafiltration. Male Wistar rats (200–230 g) received a bolus of $^{99m}$Tc-labeled compound by intravenous injection. At 3 min after the injection, the rats were anesthetized with ether and blood was collected by heart puncture. Each serum sample was prepared and applied to Centrifree units (Millipore). The units were centrifuged at 1,000*g* at room temperature. The radioactivity counts of the initial samples and filtrates were determined with an auto well γ-counter.

### Statistical Analysis

Data are expressed as means ± SD where appropriate. Results of biodistribution experiments were statistically analyzed using a 1-way ANOVA followed by the Dunnett post hoc test. Differences were considered statistically significant when *P* values were less than 0.05.

## RESULTS

### Preparation of $^{99m}$Tc-Labeled Compounds

$^{99m}$Tc-MAG3-HBP was prepared by complexation with $^{99m}$Tc using $SnCl_2$ as a reductant. The radiochemical yield of $^{99m}$Tc-MAG3-HBP was 73%. After purification by RP-HPLC, $^{99m}$Tc-MAG3-HBP had a radiochemical purity of >95%.

HYNIC-HBP, the precursor of $^{99m}$Tc-HYNIC-HBP, was synthesized by the coupling of the carboxyl group of Boc-HYNIC with the amino group of the bisphosphonate derivative and the subsequent deprotection of the Boc group. $^{99m}$Tc-HYNIC-HBP was prepared by a 1-pot reaction of HYNIC-HBP with $^{99m}TcO_4^-$, tricine, and 3-acetylpyridine in the presence of $SnCl_2$. The radiochemical yield of $^{99m}$Tc-HYNIC-HBP was 39%. After purification by RP-HPLC, $^{99m}$Tc-HYNIC-HBP had a radiochemical purity of >95%.

### Hydroxyapatite-Binding Assay

Figure 2 shows the percentage of each $^{99m}$Tc-labeled compound bound to hydroxyapatite beads. With an increase in the amount of hydroxyapatite, the rate of binding rose. Both $^{99m}$Tc-chelate−comjugated bisphosphonates ($^{99m}$Tc-MAG3-HBP and $^{99m}$Tc-HYNIC-HBP) showed a significantly higher rate of binding than $^{99m}$Tc-HMDP.

### Biodistribution Experiments

The biodistributions of $^{99m}$Tc-MAG3-HBP, $^{99m}$Tc-HYNIC-HBP, and $^{99m}$Tc-HMDP in normal rats are presented in Tables 1, 2, and 3. All $^{99m}$Tc-labeled compounds accumulated rapidly and resided a long time in the femur. $^{99m}$Tc-Chelate−conjugated bisphosphonates, $^{99m}$Tc-MAG3-HBP and $^{99m}$Tc-HYNIC-HBP, accumulated in bone in significantly larger amounts than $^{99m}$Tc-HMDP. However, the bone-to-blood ratio of $^{99m}$Tc-MAG3-HBP was decreased because its clearance from blood was delayed compared with that of $^{99m}$Tc-HMDP. $^{99m}$Tc-HYNIC-HBP had a significantly higher bone-to-blood ratio than $^{99m}$Tc-HMDP because its clearance was equivalent to that of $^{99m}$Tc-HMDP.

### Serum Protein-Binding Assay

The proportions of $^{99m}$Tc-MAG3-HBP and $^{99m}$Tc-HYNIC-HBP bound to serum protein were 97.7% ± 0.2% and 88.7% ± 2.7%, respectively.

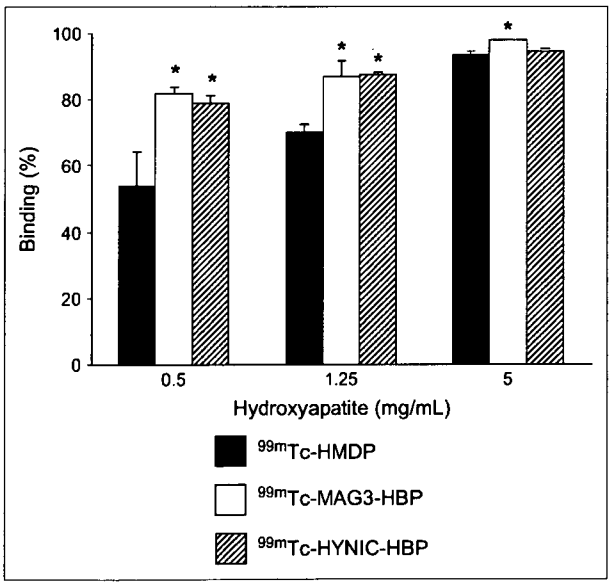


**FIGURE 2.** Binding of hydroxyapatite to $^{99m}$Tc-MAG3-HBP, $^{99m}$Tc-HYNIC-HBP, and $^{99m}$Tc-HMDP. Data are expressed as mean ± SD for 3 or 4 experiments. Asterisks indicate statistically significant differences compared with $^{99m}$Tc-HMDP with the Dunnett test ($P < 0.05$).

**TABLE 1**
Biodistribution of Radioactivity After Intravenous Administration of $^{99m}$Tc-MAG3-HBP in Rats

| Tissue | Time after administration (min) | | | |
|---|---|---|---|---|
| | 5 | 10 | 30 | 60 |
| Blood | 0.98 ± 0.09* | 0.77 ± 0.06 | 0.29 ± 0.01 | 0.07 ± 0.01* |
| Liver | 0.32 ± 0.00 | 0.29 ± 0.03 | 0.18 ± 0.01 | 0.11 ± 0.02 |
| Kidney | 2.15 ± 0.33 | 1.87 ± 0.40 | 0.85 ± 0.05* | 0.50 ± 0.08* |
| Intestine | 0.16 ± 0.03* | 0.15 ± 0.03* | 0.13 ± 0.01* | 0.17 ± 0.03* |
| Femur | 1.80 ± 0.24 | 2.31 ± 0.22 | 3.73 ± 0.18* | 4.23 ± 0.25* |
| F/B ratio† | 1.86 ± 0.38* | 3.02 ± 0.21* | 13.1 ± 0.85* | 59.7 ± 10.41 |

*Significant differences ($P < 0.05$) from $^{99m}$Tc-HMDP were identified with the Dunnett test.
†Femur-to-blood ratio.
Each value is mean ± SD for 4 animals.

## DISCUSSION

Radiopharmaceuticals with greater affinity for bone are expected to be effective in shortening the time interval between injection and bone imaging. Thus, based on the concept of bifunctional radiopharmaceuticals, $^{99m}$Tc-chelate–conjugated bisphosphonates were designed in this study. First, MAG3 was chosen as a $^{99m}$Tc-chelating group because this $N_3S$ ligand forms a relatively compact, hydrophilic, and stable complex with $^{99m}$Tc in high yields (*17*). As expected, $^{99m}$Tc-MAG3-HBP bound to the hydroxyapatite beads in vitro and accumulated in the rat femur in vivo to a greater extent than $^{99m}$Tc-HMDP. However, the level of $^{99m}$Tc-MAG3-HBP in blood was higher than that of $^{99m}$Tc-HMDP, which resulted in a decreased bone-to-blood ratio. We attribute this high radioactivity of $^{99m}$Tc-MAG3-HBP in blood to the binding of serum proteins because the $^{99m}$Tc-MAG3 complex shows strong binding to serum proteins (*18,19*). In fact, the level of binding of $^{99m}$Tc-MAG3-HBP to protein was very high.

HYNIC is a representative bifunctional chelating agent used to prepare $^{99m}$Tc-labeled proteins and peptides with tricine as a coligand (*10,20–22*). However, it has been reported that the complex [$^{99m}$Tc](HYNIC)(tricine)$_2$ is not stable and exists in multiple forms, and the pharmacokinetics could be affected by the exchange reaction between tricine and protein in the plasma and tissues (*22–24*). To solve these problems, Liu et al. used several pyridine derivatives as coligands to form ternary ligand complexes, [$^{99m}$Tc](HYNIC)(tricine)(pyridine derivative), with greater stability and fewer isomers (*25*). Furthermore, in a previous study, we showed that little binding to plasma protein was displayed by $^{99m}$Tc-HYNIC-labeled polypeptides derivatized with this ternary ligand complex (*13*). Then, $^{99m}$Tc-HYNIC-HBP in which [$^{99m}$Tc](HYNIC)(tricine)(3-acetylpyridine) was conjugated with a bisphosphonate derivative, was designed for high bone affinity and rapid washout from the blood.

The rate of binding of $^{99m}$Tc-HYNIC-HBP to serum protein was significantly lower than that of $^{99m}$Tc-MAG3-HBP. When these values were expressed as a nonprotein–binding rate, the value of $^{99m}$Tc-HYNIC-HBP (11.3%) is about 5 times the value of $^{99m}$Tc-MAG3-HBP (2.3%). The difference in the binding of the compound to the serum protein affects its blood clearance (*26–28*). In fact, the blood clearance of $^{99m}$Tc-HYNIC-HBP was significantly faster than that of $^{99m}$Tc-MAG3-HBP and was equivalent to that

**TABLE 2**
Biodistribution of Radioactivity After Intravenous Administration of $^{99m}$Tc-HYNIC-HBP in Rats

| Tissue | Time after administration (min) | | | |
|---|---|---|---|---|
| | 5 | 10 | 30 | 60 |
| Blood | 0.56 ± 0.05 | 0.39 ± 0.04* | 0.10 ± 0.01 | 0.03 ± 0.01 |
| Liver | 0.18 ± 0.02 | 0.12 ± 0.01* | 0.07 ± 0.01* | 0.05 ± 0.01 |
| Kidney | 3.19 ± 1.02 | 1.43 ± 0.09 | 0.45 ± 0.05 | 0.26 ± 0.10 |
| Intestine | 0.15 ± 0.01* | 0.10 ± 0.01 | 0.10 ± 0.07 | 0.05 ± 0.02 |
| Femur | 1.90 ± 0.21* | 2.59 ± 0.22* | 3.71 ± 0.30* | 3.96 ± 0.36* |
| F/B ratio† | 3.40 ± 0.50* | 6.69 ± 0.43 | 37.1 ± 4.01* | 123.20 ± 18.30* |

*Significant differences ($P < 0.05$) from $^{99m}$Tc-HMDP were identified with the Dunnett test.
†Femur-to-blood ratio.
Each value is mean ± SD for 6 animals.

**TABLE 3**
Biodistribution of Radioactivity After Intravenous Administration of $^{99m}$Tc-HMDP in Rats

| Tissue | Time after administration (min) | | | |
|---|---|---|---|---|
| | 5 | 10 | 30 | 60 |
| Blood | 0.61 ± 0.03 | 0.32 ± 0.04 | 0.10 ± 0.01 | 0.04 ± 0.01 |
| Liver | 0.15 ± 0.02 | 0.08 ± 0.01 | 0.03 ± 0.00 | 0.04 ± 0.05 |
| Kidney | 3.11 ± 0.23 | 1.59 ± 0.42 | 0.46 ± 0.08 | 0.24 ± 0.03 |
| Intestine | 0.12 ± 0.00 | 0.09± 0.02 | 0.04 ± 0.01 | 0.03 ± 0.01 |
| Femur | 1.52 ± 0.14 | 1.97 ± 0.18 | 2.73 ± 0.15 | 3.16 ± 0.51 |
| F/B ratio* | 2.49 ± 0.15 | 6.27 ± 0.94 | 29.16 ± 4.86 | 93.40 ± 19.81 |

*Femur-to-blood ratio.
Each value is mean ± SD for 4 or 5 animals.

of $^{99m}$Tc-HMDP, although factors other than protein binding may also be responsible for rapid blood clearance. Furthermore, $^{99m}$Tc-HYNIC-HBP accumulated in larger amounts in femur than did $^{99m}$Tc-HMDP, which could be attributable to its design based on the bifunctional radiopharmaceutical concept. Consequently, the bone-to-blood ratio of $^{99m}$Tc-HYNIC-HBP was significantly higher than that of $^{99m}$Tc-HMDP.

We assume that $^{99m}$Tc-chelate–conjugated bisphosphonates in bone remain intact because their $^{99m}$Tc complexes are stable. On the other hand, previous studies suggested that there was a separation of the $^{99m}$Tc-bisphosphonate complex into its $^{99m}$Tc and bisphosphonate components before incorporation into the mineral phase (*29,30*). However, the separation of $^{99m}$Tc-bisphosphonate must occur at the bone site because reduced $^{99m}$Tc alone was not taken up by bone (*30*). Namely, there is little difference from the point of view that bisphosphonate is used as a carrier to bone in both cases. Thus, we hypothesized that the affinity of bisphosphonate for hydroxyapatite is important for bone accumulation and it would be increased by the design of a bisphosphonate in which the phosphonate groups do not coordinate with technetium. In fact, $^{99m}$Tc-chelate–conjugated bisphosphonates had better affinity for hydroxyapatite and accumulated in the rat femur in vivo to greater extent than $^{99m}$Tc-HMDP. These results support our hypothesis. However, other factors such as the blood circulation and delivery of the agents may also be important. Further study may be required to elucidate the mechanism for bone localization.

Because MAG3-HBP and HYNIC-HBP contain a bisphosphonate site, there is the possibility that $^{99m}$Tc coordinates not with the MAG3 moiety or the HYNIC moiety but rather with the bisphosphonate moiety. To ascertain that $^{99m}$Tc is chelated with only the MAG3 moiety, Re-MAG3-HBP was prepared by the coupling of nonradioactive Re-MAG3 complexed previously with the bisphosphonate analog. By RP-HPLC analysis, identical retention times between $^{99m}$Tc-MAG3-HBP and Re-MAG3-HBP were exhibited (Fig. 3), revealing their structural analogy. In the case of the HYNIC complex, because it is difficult to synthesize the corresponding stable Re-HYNIC complex, $^{99m}$Tc-HYNIC-HBP was prepared by the coupling of [$^{99m}$Tc](HYNIC-TFP)(tricine)(3-acetylpyridine) with the bisphosphonate derivative. RP-HPLC analysis revealed this $^{99m}$Tc-labeled product to be identical to that obtained from the reaction of HYNIC-HBP with $^{99m}TcO_4^-$, tricine, and 3-acetylpyridine in the presence of $SnCl_2$ (Fig. 4). These findings exclude the possibility of complexation between technetium and the bisphosphonate structure and indicate the chelation of $^{99m}$Tc with only the MAG3 moiety in MAG3-HBP and the HYNIC moiety in HYNIC-HBP.

## CONCLUSION

As a radiopharmaceutical that accumulates at high level in bone and is rapidly cleared from blood, we designed a novel $^{99m}$Tc-chelate–conjugated bisphosphonate, $^{99m}$Tc-HYNIC-HBP. $^{99m}$Tc-HYNIC-HBP had good affinity for hydroxyapatite crystals and showed lower binding to serum proteins. In rat biodistribution experiments, $^{99m}$Tc-HYNIC-HBP had a higher bone-to-blood accumulation ratio of radioactivity at early times after injection than $^{99m}$Tc-HMDP.

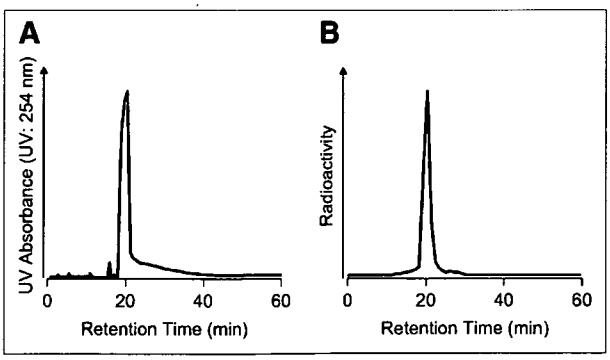


**FIGURE 3.** RP-HPLC chromatograms of nonradioactive Re-MAG3-HBP (A) and $^{99m}$Tc-MAG3-HBP (B). Conditions: flow rate of 1 mL/min with 10% ethanol in 200 mmol/L phosphate buffer (pH 6.0) containing 10 mmol/L tetrabutylammoniumhydroxide.